

Evaluation and verification of an HSDT-Layerwise Generalized Finite Element formulation for adaptive piezoelectric laminated plates

Diego Amadeu F. Torres^{1,*}, Paulo de Tarso R. Mendonça*, Clovis S. de Barcellos*

*Group of Mechanical Analysis and Design - GRANTE, Department of Mechanical Engineering,
Federal University of Santa Catarina, 88040-900,
phone: (55)(48)3721-9899, Florianópolis, SC, Brazil.*

Abstract

A formulation for the bending analysis of composite laminated plates with piezoelectric layers is implemented using the Generalized Finite Element Method. This formulation is derived from a mechanical description based on Higher-Order Shear Deformation Theory which allows for the use of C^0 continuous approximation functions on the domain. On the other hand, a Layerwise Theory is employed for interpolation of electric potential across the thickness of piezoelectric layers, in such a way that the kinematical hypotheses result in a mixed model. The paper presents an analysis of the approximation capability of the proposed numerical model for static analysis, using C^0 continuous Partition of Unity and polynomial enrichments to span the approximation spaces, by assessment of convergence. Analytical solutions obtained from the same kinematical hypotheses are used as references. Results for relative error in the energy norm considering p - and h -refinements for regular and

*Corresponding author

Email addresses: diego.amadeu@gmail.com (Diego Amadeu F. Torres),
mendonca@grante.ufsc.br (Paulo de Tarso R. Mendonça)

¹Graduate student

distorted meshes, in addition to a pointwise evaluation of the stresses and electric field, are presented. The evaluations show that the numerical methodology is a very effective tool for improving the solution through the enrichment, even for pointwise values across the thickness, and is robust to mesh distortions. Moreover, the results furnish insight about the physical modeling for both active and sensory modes, for thick and thin plates.

Keywords: GFEM, Adaptive plates, Mixed HSDT-Layerwise model, Convergence analysis

PACS:

2000 MSC:

1. Introduction

Smart/intelligent structures have received increasing attention from researchers during recent decades due to several factors. The motivation behind the use of adaptive materials is to enable a structure to change its shape or its material/structural properties, thereby improving performance and service life.

Electrostrictive materials, magnetostrictive materials, shape memory alloys, magneto or electro-rheological fluids, polymer gels, and piezoelectric materials, for example, can all be used to design and develop structures that can be called smart. However, these materials themselves are not smart. “Smartness” refers to the exploitation of material properties to better serve a design function than would be possible through conventional structural design [1].

Piezoelectric materials, among several applications, are easily integrated to structural components, when compared to adaptive materials of other categories. Because they exhibit coupled mechanical-electrical behavior, they can be used as sensors, to measure strains and acceleration, and as actuators, allowing the application of elec-

tric potential to generate a field of deformations in the structure. In this regard, they can be applied in laminated composite structures as patches and films or in the form of layers within a laminate.

During the last three decades a large variety of models have been developed to predict the behavior of piezoelectric materials in smart structures. These models may be classified into three different categories: induced strain models, coupled electromechanical models and coupled thermo-electromechanical models.

The induced strain models use theoretical approaches to consider the piezoelectric effect and they are usually limited to predicting only the active response of piezoelectric materials. In this case, the strain in the piezoelectric materials due to the applied electric potential is approximated by statically equivalent forces and moments. Even though some models have been developed with the introduction of the piezoelectric constitutive equations, allowing the sensitive behavior to be represented, the electric potential is usually not included as a state variable and is not considered in the conservation of electric flux in the displacement equations, and thus the electric voltages generated by the sensors are post-processed using the electric charge equation [2].

On the other hand, coupled electromechanical models provide a more consistent representation of both active and sensitive responses of piezoelectric materials through the incorporation of both mechanical displacements and electric potentials as state variables in the formulation. The coupled electromechanical models are the models most commonly implemented in finite element codes.

Prior to the 1990s, structures with piezoelectric devices were modeled with solid elements, following the work of Allik and Hughes [3] who formulated the dynamic equations through variational methods with the piezoelectric constitutive relations and finite element models for piezoelectric solids. However, the hexahedron or brick elements display excessive shear stiffness as the element thickness decreases. This

problem was circumvented by adding three incompatible internal degrees of freedom to the element [4]. Another approach based on solid elements was presented in [5]. Nevertheless, as a rule, the completely three-dimensional modeling of laminated piezoelectric structures results in systems with a large number of degrees of freedom, since they require one solid element per layer of the laminate.

In addition, most of the previous theories use simplifying approximations attempting to replicate the induced strain or electric fields generated by a piezoelectric layer under an external electric field or applied load.

Due the inconveniences related to fully three-dimensional modeling, the developing of two-dimensional models like plates and shells became a tendency. Hwang and Park [6] presented a two-dimensional quadrilateral plate element considering actuation by induced strain and kinematical description according the Classical Laminated Plate Theory (CLPT). Since this finite element formulation was derived considering one electrical degree of freedom, the output voltage is dependent on the integrated strain rates over the element and was calculated from the direct piezoelectric equation. When used as an actuator, the piezoelectric layer induces the control moments at the ends of the element.

Some models based on the First-Order Shear Deformation Theory (FSDT) were tested, like the ones presented in Detwiler et al. [7], for the linear response of coupled electrical-mechanical behavior, and [8], which considered the geometrical non-linearity of the structure. But, remarkably, the simple CLPT offers poor kinematic approximation capability for complex laminate systems like those equipped with piezoelectric patches.

One strategy to reduce the costs associated with full solid element models consists of the use of a Layerwise Theory (LT) to describe both mechanical and electric unknowns. Among others authors, Saravacos et al. [9] studied the complete dynamic

electromechanical response of smart piezoelectric plates under external mechanical or electric loading. Lee [2] presents a complete family of finite elements for beams, plates and shells based on LT for all state variables.

The Layerwise Theories still lead to a large number of degrees of freedom in the model when they are used for both mechanical and electrical variables, to similar extent as the full solid elements.

The particular configuration of a laminated structure with piezoelectric layers or patches makes it very difficult to adequately model with a single equivalent layer kinematic model, applied to both mechanical and electric unknowns. Therefore, a very appropriate strategy consists of using a single equivalent layer model for the mechanical unknowns and a Layerwise Theory for the electric potential. Some of the most simple of these combinations are those using the FSDT for the mechanical displacements and LT for the potential, like the shell element formulated by Saravacos [10]. Cen et al. [11] have also employed a partially hybrid energy functional for correcting the transverse shear deformation in their mixed FSDT-LT finite element formulation. In contrast, Liew et al. [12] used the mixed FSDT-LT models in a formulation based on the Element-Free Galerkin Method.

It is well known that the FSDT also results in some deficiencies in the approximation of the mechanical response of anisotropic laminates, particularly in underestimating displacements and providing poor transverse shear stress results. The Higher-Order Shear Deformation Theories (HSĐT), for example [13] [14] [15], behave much better and several researches indicate that they represent a good choice for the mechanical displacements in an piezoelectric laminate, combined with the LT for the electric potential. This can be seen in the work of Reddy [16] [17], Chee [18] and Faria [19], among others.

Firstly, [16] presented a hybrid kinematical hypothesis, and corresponding ana-

lytical solutions, based on an equivalent single layer theory, Reddy's Higher-Order Shear Deformation Theory (HSDT) [13], for the mechanical displacements and layerwise discretization of the electric potential. [17] also derived a theoretical formulation of the Navier solutions of simply supported rectangular laminates and displacement finite element models for laminated composite plates with integrated sensors and actuators. The CLPT, Higher-Order Shear Deformation Theory [13] and thermo-electric mechanical coupling were also considered using piecewise linear functions across the thickness to approximate temperature and electric fields.

It should be noted that Reddy's HSDT essentially generates a C^1 -continuous formulation, but most of the finite element formulations are based on C^0 -continuous shape functions and therefore requires some especial treatment.

Following this tendency, [18] and [19] also implemented finite elements based on HSDT [15] and LT, using C^0 -continuous shape functions. A similar approach was used in [20], which also presents a strong formulation for the problem, and performed some optimization analysis of piezoelectric structural configurations.

A more elaborate kinematical hypothesis is proposed in [21], who presented a finite element formulation based on a fourth-order expansion through the laminate thickness, combined with a piecewise linear term to describe the mechanical variables and a quadratic distribution of the electric potential inside each piezoelectric layer.

On the other hand, a fully layerwise description was implemented in [22] using Lagrange polynomials within each layer. Although traditional layerwise theories are able to accurately predict stress, electrical displacements, mechanical displacements and electric potential, they are unable to guarantee the continuity of transverse stresses and transverse electrical displacement (when there are stacked piezoelectric layers). Following [23], who used a Reissner variational principle with a layerwise description, [24] developed a layerwise formulation for piezolaminated plates based

on a mixed variational principle, in such a way that interfacial conditions of stress and electrical displacement are directly imposed. [25] extended the formulation of [24] to incorporate the magneto-electro-elastic phenomenon also using a partially hybrid functional with higher-order functions across the thickness based on a complete layerwise description.

The present paper develops a procedure to numerically analyze the coupled electro-structural response of laminated plates with orthotropic fiber reinforced layers and piezoelectric layers, using the Generalized Finite Element Method (GFEM). The mechanical unknowns, the displacements, are modeled by a higher-order shear deformation theory (HSDT) of the third-order [14] which allows for the use of C^0 -continuous approximation functions. The electric unknowns, the potentials, are modeled by a Layerwise Theory, utilizing piecewise linear functions across the thickness of piezoelectric layers. All fields are enriched according to the Generalized Finite Element Method, utilizing polynomial enrichment functions applied to a bilinear Partition of Unity defined on each element and the main focus is to verify the performance of the numerical method. The remainder of this paper is outlined as follow: Section 2 provides a review of the GFEM basics. Section 3 deals with the linear electro-elasticity formulation. Section 4 details the proposed application of the GFEM strategy to the problem of laminated plates with orthotropic piezoelectric layers, showing the discretization, the global enrichment of the approximating spaces, stiffness and inertia matrices, mechanical-electrical coupling matrices and mechanical and electric dynamic load vectors. Section 5 presents a strong formulation for the problem under analysis, from which analytical solutions may be obtained. Section 6 shows numerical applications for static analysis of laminated plates with piezoelectric layers considering both active and sensory modes, presents a convergence analysis using a global measure of the relative error in energy norm and pointwise assess-

ment of the stress and electric field for comparison with the analytical solutions, and Section 7 summarizes some conclusions.

2. Generalized Finite Element Method

A hybrid method combining the *hp* Clouds Method and the conventional form of the Finite Element Method was presented by [26]. This strategy takes into account the idea of adding hierarchical refinements to a set of shape functions associated with finite elements, such as the Lagrangian interpolations, for example, which satisfy the requirement of a Partition of Unity (PoU). This procedure allows the construction of richer ansatz spaces for approximate solutions of partial differential equations (PDEs).

The resultant methodology, established in [27], [28], and [29], called Generalized Finite Element Method (GFEM) could be mentioned in the context of the Meshfree Methods.

In Meshfree methods, the approximation of field variables is constructed in terms of nodes without the aid of a mesh. Due to the flexibility in constructing conforming shape functions to meet specific needs for different applications, Meshfree methods are particularly suitable for *hp*-adaptivity, simulation of crack propagation and large deformation problems, among others [30]. However, they require the partition of the domain through the use of a “background grid” for domain integration. Hence, one of the main drawbacks of Meshfree methods is that the computational cost is too high in some applications due to the fact that one has to use a great number of integration points in order to perform the domain integration accurately [31]. Moreover, it must be guaranteed that the weighted moment matrix derived in the construction of approximation functions by the Moving Least Square Method is invertible, which is related to the nodal density [32].

In the GFEM context, discretization spaces for a Galerkin method are defined using the concept of the Partition of Unit Finite Element Method (PUFEM), [33], [34], [35], [36], and of the hp Clouds Method, [37] and [38].

The GFEM is one of the instances of the Partition of Unity Method and allows a simple and effective scheme for tailoring the approximation functions for each kind of problem. In this context, a mesh of elements is created to perform the following operations: (a) to facilitate the numerical integration; and (b) to define the PoU locally within elements by intrinsic coordinates. Finally, the PoU functions are externally enriched by functions defined in global coordinates. This last aspect is responsible for the high efficiency of the method.

Usually the enrichment functions are polynomials, but special enrichment functions can be used to provide more accurate and robust simulations since, through this framework, it is possible to use compactly supported non-polynomial bases in the solution space. These functions can be built based on *a-priori* knowledge regarding the analytical expressions which reflect the nature of the solution of a problem, like crack modeling [39], as well as based on the solution of local boundary value problems, for instance, in global-local strategies [40] or the mesh-based handbook function generated from canonical domains containing microstructural features [41].

In recent years, the GFEM has been applied to a diversity of phenomena such as the analysis of dynamic crack propagation [42] and materials with internal cracks [29] and voids [41]. It has also being used to build arbitrarily smooth approximations for handling higher-order distributional boundary conditions [30]. [43] uses it to perform *a posteriori* error estimation and p -adaptive analysis using C^k base functions. [44] address the *a posteriori* error estimation using mesh-based handbook functions as enrichments for materials with many voids. [45] and [40] use a global-local strategy in GFEM for heat transfer with high gradients. [46] develops a C^k continuous finite

element formulation for the *Kirchhoff* laminate model. A procedure to define richer approximate subspaces for shell structures and the treatment for boundary layer phenomenon is addressed by [47].

Partition of Unity (PoU) is a set of functions for which the sum of their values is equal to unity on every point of the support. Besides this aspect, three other characteristics are used to verify the applicability of this definition to a set of basis functions. According to [48], over an open bounded domain Ω in R^n , with a countable open covering constructed with a countable collection of open sets $\{G_j\}$ such that $\Omega \subset \bigcup_{j=1}^N G_j$, a collection of functions $\varphi_j(\mathbf{x})$ forms a Partition of Unity if it has the following properties:

- $\varphi_j(\mathbf{x}) \in C_0^\infty(G_j);$
- $\sum_{j=1}^N \varphi_j(\mathbf{x}) = 1;$
- $\varphi_j(\mathbf{x}) \geq 0$ em Ω ;
- every compact subset of Ω intersects only a finite number of the supports of the $\varphi_j(\mathbf{x})$.

The first one is usually relaxed to $C_0^k(G_j)$ for some $k \geq 0$.

It should be noted that the standard finite element shape functions form a Partition of Unity. In general, the GFEM can be briefly defined as a strategy to enlarge the FEM approximation space by adding special functions to the conventional approximation basis. This basis now takes the role of a Partition of Unity and allows inter-element continuity and creates conforming approximations. The enrichment allows the application of any information that reflect previous knowledge on the boundary value problem solution, such as a singular function resulting from local

asymptotic expansion of the exact solution close to a point. The approximating capabilities of the enrichment functions are included in the function space of the method while keeping the same standard structure of an FEM code.

For instance, the GFEM local approximation capability can be described as follows. Let a function u be defined over the domain Ω covered by the clouds. Let \tilde{u}_j^i be a local approximation of u which belongs to a local subspace $\mathcal{X}_j(\omega_j)$ defined over the cloud support ω_j , such that $\mathcal{X}_j(\omega_j) = \text{span}\{\mathcal{L}_{ji}\}_{i \in \jmath(j)}$, where $\jmath(j)$, $j = 1, 2, \dots, N$, is the index set which refers to the enrichment functions associated with each node, \mathcal{L}_{ji} denotes an enrichment function i related to the node \mathbf{x}_j and N is the number of nodes of the connected domain.

Basically, GFEM proposes that each subspace $\mathcal{X}_j(\omega_j)$ may be chosen in such a way that $\mathcal{L}_{ji} \in \mathcal{X}_j(\omega_j)$ can closely approximate $u|_{\omega_j}$ over the cloud ω_j , without compromising the conforming requirement.

The cloud functions family $\mathcal{F}_N^{k,p}$ is composed of the PoU, which generates the polynomial space of degree k , \mathcal{P}_k , and is endowed with the capability of representing exactly the polynomials of the space of degree p , \mathcal{P}_p . It is defined by

$$\mathcal{F}_N^{k,p} = \left\{ \{\varphi_j(\mathbf{x})\}_{j=1}^N \bigcup \{\varphi_j(\mathbf{x})\mathcal{L}_{ji}(\mathbf{x})\}_{j=1}^N \mid i \in \jmath(j) \right\} \quad (1)$$

where $\varphi_j(\mathbf{x})$ are PoU functions and $\mathcal{L}_{ji}(\mathbf{x})$ are the enrichment functions, both related to the node j , and $\jmath(j)$ is an index set which refers to the enrichment functions associated with each node. Presently

$$\mathcal{F}_N^{k,p} = \begin{Bmatrix} \varphi_1 1 & \varphi_2 1 & \cdots & \varphi_N 1 \\ \varphi_1 \mathcal{L}_{11} & \varphi_2 \mathcal{L}_{21} & \cdots & \varphi_N \mathcal{L}_{N1} \\ \vdots & \vdots & \vdots & \vdots \\ \varphi_1 \mathcal{L}_{1M} & \varphi_2 \mathcal{L}_{2M} & \cdots & \varphi_N \mathcal{L}_{NM} \end{Bmatrix} \quad (2)$$

where N is the number of clouds and p is the dimension of the highest complete polynomial space spanned by $\mathcal{F}_N^{k,p}$ and M is the number of enrichment functions related to the nodes.

This cloud family is used to build the following approximation

$$\tilde{u}(\mathbf{x}) = \sum_{j=1}^N \varphi_j(\mathbf{x}) \left\{ u_j + \sum_{i=1}^{q_j} \mathcal{L}_{ji}(\mathbf{x}) b_{ji} \right\} = \Phi^T \mathbf{U} \quad (3)$$

with

$$\mathbf{U}^T(\mathbf{x}) = \begin{bmatrix} u_1 & b_{11} & \cdots & b_{1q_j} & \cdots \\ \cdots & u_N & b_{N1} & \cdots & b_{Nq_j} \end{bmatrix} \quad (4)$$

where u_j and b_{ji} are the nodal parameters associated with the standard finite element shape functions $\varphi_j(\mathbf{x})$, and to the enriched functions $\varphi_j(\mathbf{x})\mathcal{L}_{ji}(\mathbf{x})$, respectively, grouped in the vector

$$\Phi^T = \begin{bmatrix} \varphi_1 & \mathcal{L}_{11}\varphi_1 & \cdots & \mathcal{L}_{1q_j}\varphi_1 & \cdots \\ \varphi_N & \mathcal{L}_{N1}\varphi_N & \cdots & \mathcal{L}_{Nq_j}\varphi_N \end{bmatrix} \quad (5)$$

where q_j is the number of enrichment functions of each node.

Let \mathcal{U} and $\mathcal{V} \in \mathcal{H}^1(\Omega)$ be *Hilbert* spaces of degree 1, which are standard Sobolev spaces of square integrable functions whose first derivatives are also square integrable (in the sense of Lebesgue), and which are defined on the domain Ω . Consider the boundary value problem of finding $u \in \mathcal{U}$ such that $\mathcal{B}(u, v) = \mathcal{L}(v)$, $\forall v \in \mathcal{V}$.

Now let \mathcal{U}_h be the subspace spanned by a set of kinematically admissible functions and \mathcal{V}_h the subspace spanned by a set of kinematically admissible variations. We define the following *Galerkin* approximation, in the GFEM approach, for the

boundary value problem, which consists of: find $\tilde{u} \in \mathcal{U}_h$ such that $\mathcal{B}(\tilde{u}, \tilde{v}) = \mathcal{L}(\tilde{v})$, $\forall \tilde{v} \in \mathcal{V}_h$, where \tilde{u} and $\tilde{v} \in \mathcal{U}_h = \mathcal{V}_h \subset \mathcal{H}^1$, $\mathcal{B}(\bullet, \bullet)$ is a bilinear form of $\mathcal{H}^1 \times \mathcal{H}^1 \rightarrow \mathbb{R}$ and $\mathcal{L}(\bullet)$ a linear form of $\mathcal{H}^1 \rightarrow \mathbb{R}$, leading to the discrete form $\mathcal{B}(\Phi^T \mathbf{U}, \Phi^T \mathbf{V}) = \mathcal{L}(\Phi^T \mathbf{V})$ where

$$\mathbf{V}^T = \begin{bmatrix} v_1 & c_{11} & \cdots & c_{1q_j} & \cdots \\ & v_N & c_{N1} & \cdots & c_{Nq_j} \end{bmatrix} \quad (6)$$

are nodal parameters related to the test function, such that $\Phi^T \mathbf{V} \in \mathcal{V}_h$.

In the present work, the PoU is defined by bilinear Lagrangian shape functions and, without loss of generality, only polynomial enrichment up to the third degree is used, according to the following linear combinations

$$\varphi_j \times \left\{ 1, \frac{x - x_j}{h_{x_j}}, \frac{y - y_j}{h_{y_j}}, \left(\frac{x - x_j}{h_{x_j}} \right)^2, \left(\frac{x - x_j}{h_{x_j}} \right) \left(\frac{y - y_j}{h_{y_j}} \right), \dots, \left(\frac{y - y_j}{h_{x_j}} \right)^3 \right\} \quad (7)$$

where φ_j , $j = 1, 2, \dots, N$, are standard FEM bilinear shape functions, $\mathbf{x}_j = (x_j, y_j)$ are nodal coordinates of an arbitrary node j , h_{x_j} and h_{y_j} are the cloud characteristic dimensions of the node in the directions x and y , respectively, and N is the number of nodes of the finite element mesh. Consequently, $k = 1$, $p = 4$ and $\mathcal{J}(j) = \{1, 2, \dots, 10\}$.

It can be noted that by using this enrichment procedure only the PoU satisfies the Kronecker delta condition, i.e., $\varphi_j(x_i) = \delta_{ij}$, since the enriched functions associated with a given node are zero at this node. Therefore, the Dirichlet boundary conditions cannot be directly imposed, a special procedure being required to impose

them. For instance, one efficient procedure to impose essential boundary conditions is through the so-called boundary functions, as proposed in [47], which allows an adequate enrichment in the boundary vicinity while preserving the completeness of the polynomials that span the approximation subspace.

In spite of this, once a displacement component u is defined over a cloud j as

$$u = u_j \varphi_j + b_{j1} (\varphi_j \mathcal{L}_{j1}) + b_{j2} (\varphi_j \mathcal{L}_{j2}) + \cdots + b_{j9} (\varphi_j \mathcal{L}_{j9}) \quad (8)$$

it is possible, for boundaries parallel to the axis of the global problem coordinates, to use a simplified method to enforce essential boundary conditions. For instance, for nodes on a boundary line $x = \text{const.}$ one may enforce the condition $u = 0$ by just making the following parameters null

$$u_j = b_{j2} = b_{j5} = b_{j9} = 0 \quad (9)$$

On the other hand, for a boundary line $y = \text{const.}$ and the same condition $u = 0$, one must impose

$$u_j = b_{j1} = b_{j3} = b_{j6} = 0 \quad (10)$$

For non-homogeneous Dirichlet boundary conditions $u = \bar{u}$ one can impose $u_j = \bar{u}$ in strong form making all the other nodal parameters null.

3. Constitutive equations

The coupling between the mechanical, thermal and electric fields can be established using thermodynamic principles and the Maxwell relations [49]. Analogously to the deformation energy functional U_0 , in the linear elasticity theory, and the

Helmholtz free energy functional Ψ_0 , in thermoelasticity, the existence of a functional Φ_0 it is assumed such that

$$\begin{aligned}\Phi_0(\varepsilon_{ij}, E_i, \phi) &= U_0 - \mathbf{E} \cdot \mathbf{D} - \eta\phi \\ &= \frac{1}{2}C_{ijkl}\varepsilon_{ij}\varepsilon_{kl} - e_{ijk}\varepsilon_{ij}E_k - \beta_{ij}\varepsilon_{ij}\phi \\ &\quad - \frac{1}{2}\chi_{kl}E_kE_l - p_kE_k\phi - \frac{\rho c_v}{2\phi_0}\phi^2\end{aligned}\tag{11}$$

denoted the *Gibbs free energy functional*. Here, η is the enthalpy, C_{ijkl} are the elastic moduli, e_{ijk} are the piezoelectric moduli or, more precisely, the constants of piezoelectric deformation, χ_{ij} are the dielectric constants, p_k are the pyroelectric constants, β_{ij} are stress-temperature expansion coefficients, c_v is the specific heat at constant volume, per unit mass, ϕ is the temperature, and ϕ_0 is the absolute reference temperature. Differentiation of this functional with respect to the fields ε , \mathbf{E} and ϕ results in the coupled constitutive relations for a deformable pyro-piezoelectric material, as can be seen in [49].

The formulation derived in the present paper ignores variations in temperature such that the coupled equations become

$$\begin{aligned}\sigma_i &= C_{ij}^E\varepsilon_j - e_{ik}E_k \\ D_k &= e_{kj}\varepsilon_j + \chi_{kl}^E E_l \\ \eta &= \beta_j\varepsilon_j + p_kE_k\end{aligned}\tag{12}$$

where σ_{ij} are the components of the Cauchy stress tensor, D_i are the components of the electric displacement vector and η is the enthalpy. In (12) the contracted notation was used, taking into account the symmetry of stress and strain tensors, such that the stress components are organized in vector form as $\boldsymbol{\sigma} = \{ \sigma_x \sigma_y \sigma_z \tau_{yz} \tau_{xz} \tau_{xy} \}^T$. The same operation is performed for the deformation components. The enthalpy

becomes uncoupled from the other fields, and the solution is obtained from the first two equations. These relations can be reordered into one single matrix relation, linear and electromechanically coupled, in the orthotropic material directions, along axes 1, 2 and 3

$$\begin{Bmatrix} \boldsymbol{\sigma}^1 \\ \mathbf{D}^1 \end{Bmatrix}^k = \begin{bmatrix} \mathbf{C}^1 & -\mathbf{e}^{1T} \\ \mathbf{e}^1 & \boldsymbol{\chi}^1 \end{bmatrix}^k \begin{Bmatrix} \boldsymbol{\varepsilon}^1 \\ \mathbf{E}^1 \end{Bmatrix}^k \quad (13)$$

where the superscript 1 indicates the material coordinate system and k is the number of an arbitrary piezoelectric layer. For the piezoelectric extensional mode of actuation, only the following coefficients in (13) are non-zero: $C_{11}^1, C_{12}^1, C_{13}^1, C_{21}^1, C_{22}^1, C_{23}^1, C_{33}^1, C_{44}^1, C_{55}^1$ and C_{66}^1 , for the 6×6 stiffness matrix \mathbf{C}^1 ; $e_{15}^1, e_{24}^1, e_{31}^1, e_{32}^1$ and e_{33}^1 , for the 3×6 piezoelectric matrix \mathbf{e}^1 ; and χ_{11}^1, χ_{22}^1 and χ_{33}^1 for the 3×3 dielectric matrix $\boldsymbol{\chi}^1$.

In this formulation, each composite layer is considered to be orthotropic, whether it is piezoelectric or not. Therefore, the constitutive relation (12) must be rotated to the global laminate coordinate system, according to the layer orientation angle, and then it is combined into the laminate constitutive relation. The stress vector after axes rotation $\boldsymbol{\sigma}^x$ is given by

$$\boldsymbol{\sigma}^x = \mathbf{T} \left(\mathbf{C}^1 \mathbf{R} \mathbf{T}^{-1} \mathbf{R}^{-1} \boldsymbol{\varepsilon}^x - \mathbf{e}^{1T} \mathbf{L} \mathbf{E}^x \right) \quad (14)$$

where the superscript T indicates a transposed matrix. Through an analogous procedure one obtains the rotated electric displacement vector \mathbf{D}^x

$$\mathbf{D}^x = \mathbf{L}^T \left(\mathbf{e}^1 \mathbf{R} \mathbf{T}^{-1} \mathbf{R}^{-1} \boldsymbol{\varepsilon}^x + \boldsymbol{\chi}^1 \mathbf{L} \mathbf{E}^x \right) \quad (15)$$

where \mathbf{T} , \mathbf{R} and \mathbf{L} are defined as follows

$$\mathbf{T} = \begin{bmatrix} c^2 & s^2 & 0 & 0 & 0 & -2sc \\ s^2 & c^2 & 0 & 0 & 0 & 2sc \\ 0 & 0 & 1 & 0 & 0 & 0 \\ 0 & 0 & 0 & c & s & 0 \\ 0 & 0 & 0 & -s & c & 0 \\ sc & -sc & 0 & 0 & 0 & c^2 - s^2 \end{bmatrix} \quad (16)$$

where $s = \sin \theta$, $c = \cos \theta$, with θ being the rotation angle between principal axis 1 and global axis x, in a counter-clockwise rotation around the transverse axis 3.

Moreover, $\mathbf{R} = \text{diag} \begin{bmatrix} 1 & 1 & 1 & 2 & 2 & 2 \end{bmatrix}$. Finally,

$$\mathbf{L} = \begin{bmatrix} \cos \theta & \sin \theta & 0 \\ -\sin \theta & \cos \theta & 0 \\ 0 & 0 & 1 \end{bmatrix} \quad (17)$$

In addition, for simple monolithic piezoelectric materials polarized along the principal transverse direction 3, the piezoelectric properties would be the same in both the 1 and 2 in-plane directions. The two piezoelectric constants that are usually tabulated are d_{31} and d_{33} (in the strain formulation) - the first subscript indicates the direction of the electric field and the second subscript the direction of the strain. It can be shown that the material parameters are interrelated by $d_{mi} = e_{mi} C_{li}$.

4. GFEM formulation for the problem

In this section, a generalized finite element is implemented to model laminated plates with piezoelectric sensors and actuators. The domain is partitioned into quadrilateral elements defined by 8 nodes and corresponding standard biquadratic Serendipity functions. The Partition of Unity is defined by the four vertex nodes and

the corresponding Lagrangian bilinear functions which are, in turn, enriched according to the GFEM procedure in order to generate the enriched space of approximation for the unknown electric and mechanical fields.

The formulation used here is derived from the Hamilton's Principle, where the Hamiltonian is built in such a way to be variationally equivalent to the differential governing equations of the mechanical and electrical responses in an electromechanically coupled continuum [2]. These equations are the *Cauchy's equations of motion*,

$$\frac{\partial \sigma_{ij}}{\partial x_j} + f_i = \rho \ddot{u}_i \quad (18)$$

(where the summation convention is used) and the *Maxwell's equations of conservation of electric flux*

$$\frac{\partial D_i}{\partial x_i} = Q \quad (19)$$

where σ_{ij} are Cartesian components of stress tensor, f_i are components of body force per unit volume, ρ is the specific mass per unit volume of the material, u_i are components of mechanical displacement, D_i are components of electric displacement (electric flux) and q is the electric charge.

The functional of the Hamilton's Principle is [18]

$$\int_{t_0}^{t_1} (\delta K - \delta P + \delta W) dt = 0 \quad (20)$$

which must hold for any $t_1 > t_0$, where K , P and W are the total kinetic energy, the total deformation energy and the total work of external forces applied to the system, respectively, and δ is the variation operator. The expression can be expanded as

$$\begin{aligned}
& \int_{t_0}^{t_1} \left\{ - \int_V \rho \delta \mathbf{u}^T \ddot{\mathbf{u}}(\mathbf{x}, t) dV - \int_V \left\{ \begin{array}{c} \sigma^x \\ \mathbf{D}^x \end{array} \right\}^T \left\{ \begin{array}{c} \delta \epsilon^x \\ -\delta \mathbf{E}^x \end{array} \right\} dV + \right. \\
& \quad \left. + \int_V \delta \mathbf{u}^T \mathbf{b}^V dV + \int_S \delta \mathbf{u}^T \mathbf{f}^S dS + \delta \mathbf{u}^T \mathbf{f}^P \right. \\
& \quad \left. + \int_V \delta \varphi^T Q dV - \int_S \delta \varphi^T q dS \right\} dt = 0
\end{aligned} \tag{21}$$

where \mathbf{u} is the vector of mechanical displacement, $\boldsymbol{\sigma}$ is the Cauchy stress tensor, $\boldsymbol{\epsilon}$ is the linear strain tensor, \mathbf{D} is the electric displacement, \mathbf{E} is the electric field, \mathbf{f}^S is surface force, \mathbf{f}^V body force, \mathbf{f}^P are concentrated forces, φ is the electric potential, Q is a free electric charge and q is a free electric charge at the surface. The components of the stress and strain tensors appear in the equation organized in vector form.

The mechanical behavior of the plate undergoing bending is modeled by the Equivalent Single Layer (ESL) methodology, using the kinematical hypothesis following Levinson's Higher-Order Shear Deformation Theory [14]. Hence, the present formulation is based on following assumed displacement field

$$\begin{aligned}
u(\mathbf{x}, t) &= u^0(x, y, t) + z\psi_x(x, y, t) + z^3\psi_{3x}(s, y, t) \\
v(\mathbf{x}, t) &= v^0(x, y, t) + z\psi_y(x, y, t) + z^3\psi_{3y}(x, y, t) \\
w(\mathbf{x}, t) &= w^0(x, y, t)
\end{aligned} \tag{22}$$

where (u, v, w) are the components, in the Cartesian directions, of the displacement of an arbitrary point in the laminated plate. This theory is chosen here due its relatively lower computational cost, since only 7 generalized displacements are required, u^0 , v^0 , w^0 , ψ_x , ψ_y , ψ_{3x} and ψ_{3y} . u^0 , v^0 and w^0 are the displacements of a point in the reference plane, ψ_x and ψ_y are rotations of a segment normal to the middle plane around the

y -axis and x -axis, respectively, and ψ_{3x} and ψ_{3y} are higher-order warping variables in the $x - z$ and $y - z$ -planes, respectively. These are the mechanical unknown fields that can be approximated over the bi-dimensional (x, y) domain through function spaces with C^0 continuity.

The choosing of a thin or thick plate model is a decision which cannot be made *a priori* because it depends on the solution and the goals of the computation, for example, the calculation of displacements or stresses. Moreover, according to [50], hierachic plate/shell models $(HM|i)$, with order i , have the property

$$\lim_{i \rightarrow \infty} \|u_{EX}^{3D} - u_{EX}^{(HM|i)}\|_{E(\Omega)} \leq Cd^{\alpha_i} \quad (23)$$

when u_{EX}^{3D} , the fully three-dimensional solution, is smooth. In (23), C is a constant, independent of i , α_i is a constant which depends on i , and $\alpha_{i+1} > \alpha_i$. Thus, HSDT has a higher rate of convergence than FSDT or CLPT.

Using the linear strain-displacement relations it is possible to obtain the strain field, which is separated into *coplanar strains* $\boldsymbol{\varepsilon}_{mf}(\mathbf{x}, t)$

$$\begin{aligned} \boldsymbol{\varepsilon}_{mf}(\mathbf{x}, t) = & \left\{ \begin{array}{l} \varepsilon_x(\mathbf{x}, t) \\ \varepsilon_y(\mathbf{x}, t) \\ \gamma_{xy}(\mathbf{x}, t) \end{array} \right\} = \left\{ \begin{array}{l} \frac{\partial u^0}{\partial x} \\ \frac{\partial v^0}{\partial y} \\ \frac{\partial u^0}{\partial y} + \frac{\partial v^0}{\partial x} \end{array} \right\} \\ & + z \left\{ \begin{array}{l} \frac{\partial \psi_x}{\partial x} \\ \frac{\partial \psi_y}{\partial y} \\ \frac{\partial \psi_x}{\partial y} + \frac{\partial \psi_y}{\partial x} \end{array} \right\} + z^3 \left\{ \begin{array}{l} \frac{\partial \psi_{3x}}{\partial x} \\ \frac{\partial \psi_{3y}}{\partial y} \\ \frac{\partial \psi_{3x}}{\partial y} + \frac{\partial \psi_{3y}}{\partial x} \end{array} \right\} \end{aligned} \quad (24)$$

where it is possible to identify the *generalized extensional strains*, $\boldsymbol{\varepsilon}^0$, the *generalized*

flexural rotations, κ_1 , and the *generalized warp rotations*, κ_3 , such that

$$\boldsymbol{\varepsilon}_{mf}(\mathbf{x}, t) = \boldsymbol{\varepsilon}^0(x, y, t) + z\kappa_1(x, y, t) + z^3\kappa_3(x, y, t) \quad (25)$$

The *transverse shear strains*, $\gamma_c(\mathbf{x}, t)$, are given by

$$\begin{aligned} \boldsymbol{\gamma}_c(\mathbf{x}, t) &= \left\{ \begin{array}{l} \gamma_{yz}(\mathbf{x}, t) \\ \gamma_{xz}(\mathbf{x}, t) \end{array} \right\} \\ &= \left\{ \begin{array}{l} \psi_y + \frac{\partial w^0}{\partial y} \\ \psi_x + \frac{\partial w^0}{\partial x} \end{array} \right\} + 3z^2 \left\{ \begin{array}{l} \psi_{3y} \\ \psi_{3x} \end{array} \right\} \end{aligned} \quad (26)$$

where it is possible identify the *generalized shear strains*, $\boldsymbol{\gamma}^0$, and the *generalized shear-warp strains*, $\boldsymbol{\kappa}_2$, such that

$$\boldsymbol{\gamma}_c(\mathbf{x}, t) = \boldsymbol{\gamma}^0(x, y, t) + 3z^2\boldsymbol{\kappa}_2(x, y, t) \quad (27)$$

In this stage, it is necessary to define how the electric degrees of freedom are incorporated. Reddy's Layerwise Theory [49] is adopted here for interpolation of the electric potential field. The electric potential in the element, $\varphi(\mathbf{x}, t)$, is approximated by piecewise functions across the piezoelectric layer thicknesses. This hypothesis is acceptable since the voltage is generally applied parallel to the active layer, assuming homogeneous material.

According to these laminate theories, each layer is modeled using independent approximations for the in-plane displacement components and the electrostatic potential, in a unified representation, in accordance with the linear theory of piezoelectricity.

Consider a laminate with n_{piez} piezoelectric layers. To each arbitrary node no on the laminate middle plane corresponds $N = n_{piez} + 1$ electric potential nodal values, φ_{no}^1 to φ_{no}^N , if such piezoelectric plies are contiguous or $N = 2n_{piez}$ electric potential nodal values if there is inert material between them. Hence the potential approximation $\tilde{\varphi}_{no}^k$ in an intermediary position z within an arbitrary piezoelectric layer k in the instant t is given by the expression

$$\tilde{\varphi}_{no}^k(z, t) = \varphi_{no}^{k-1}(t) \zeta_{k-1} + \varphi_{no}^k(t) \zeta_k \quad (28)$$

with

$$\zeta_{k-1} = \left(\frac{z_k - z}{h_k} \right) \quad \text{and} \quad \zeta_k = \left(\frac{z - z_{k-1}}{h_k} \right) \quad (29)$$

Other important aspect, which is an inherent limitation related to the HSDT model used here, is that both σ_3^x and ε_3^x are assumed to vanish. Hence, similarly to the correction proposed by [51] for their model based on the FSDT, the imposition of the condition $\sigma_3^x = 0$, with the elimination of ε_3^x , leads to a reduced version of the constitutive relations, where the new coefficients are

$$\begin{aligned}
C_{11} &= \bar{C}_{11} - \frac{(\bar{C}_{13})^2}{\bar{C}_{33}} & C_{12} &= \bar{C}_{12} - \frac{\bar{C}_{13}\bar{C}_{23}}{\bar{C}_{33}} \\
C_{16} &= \bar{C}_{16} - \frac{\bar{C}_{13}\bar{C}_{36}}{\bar{C}_{33}} & C_{22} &= \bar{C}_{22} - \frac{(\bar{C}_{23})^2}{\bar{C}_{33}} \\
C_{26} &= \bar{C}_{26} - \frac{\bar{C}_{23}\bar{C}_{36}}{\bar{C}_{33}} & C_{66} &= \bar{C}_{66} - \frac{(\bar{C}_{36})^2}{\bar{C}_{33}} \\
C_{44} &= \bar{C}_{44} & C_{45} &= \bar{C}_{45} & C_{55} &= \bar{C}_{55}
\end{aligned} \tag{30}$$

$$\begin{aligned}
e_{14} &= \bar{e}_{14} & e_{15} &= \bar{e}_{15} & e_{24} &= \bar{e}_{24} & e_{25} &= \bar{e}_{25} \\
e_{31} &= \bar{e}_{31} + \frac{\bar{C}_{13}\bar{e}_{33}}{\bar{C}_{33}} & e_{32} &= \bar{e}_{32} + \frac{\bar{C}_{23}\bar{e}_{33}}{\bar{C}_{33}} \\
e_{36} &= \bar{e}_{36} + \frac{\bar{e}_{33}\bar{C}_{36}}{\bar{C}_{33}}
\end{aligned}$$

$$\begin{aligned}
\chi_{11} &= \bar{\chi}_{11} & \chi_{12} &= \bar{\chi}_{12} & \chi_{22} &= \bar{\chi}_{22} \\
\chi_{33} &= \bar{\chi}_{33} + \frac{(\bar{e}_{33})^2}{\bar{C}_{33}}
\end{aligned}$$

where the barred quantities \bullet are the coefficients obtained from the property matrices after axis rotation.

The GFEM formulation is implemented beginning with the definition of the Partition of Unity (PoU) functions over the element domain. The enrichment is made adding new parameters linked to unknown nodal values which are associated with the functions that multiply the original PoU functions. In this way, the generalized mechanical displacements over the laminate middle plane, $(u^0, v^0, w^0, \psi_x, \psi_y, \psi_{3x}, \psi_{3y})$, can be approximated, for instance, as

$$\begin{aligned}
\tilde{u}^0 &= \sum_{no=1}^{Nne} \mathbb{N}_{no}^e(x, y) \left(u_{no}^0(t) + \sum_{j=1}^{nf(u_{no}^0)} u_{no}^{0j}(t) f_{u_{no}^0}^j(x, y) \right) \\
\tilde{v}^0 &= \sum_{no=1}^{Nne} \mathbb{N}_{no}^e(x, y) \left(v_{no}^0(t) + \sum_{j=1}^{nf(v_{no}^0)} v_{no}^{0j}(t) f_{v_{no}^0}^j(x, y) \right) \\
\tilde{w}^0 &= \sum_{no=1}^{Nne} \mathbb{N}_{no}^e(x, y) \left(w_{no}^0(t) + \sum_{j=1}^{nf(w_{no}^0)} w_{no}^{0j}(t) f_{w_{no}^0}^j(x, y) \right) \\
&\vdots \\
\tilde{\psi}_{3y} &= \sum_{no=1}^{Nne} \mathbb{N}_{no}^e(x, y) \left(\psi_{3y_{no}}(t) + \sum_{j=1}^{nf(\psi_{3y_{no}})} \psi_{3y_{no}}^j(t) f_{\psi_{3y_{no}}}^j(x, y) \right)
\end{aligned} \tag{31}$$

where $\mathbb{N}_{no}^e(x, y)$ is the portion of the PoU functions matrix related to the node no , Nne stands for the number of nodes and $nf(\bullet_{no})$ denotes the number of enrichment functions associated with the unknown \bullet at node no . Hence, by assembling all the functions in a single matrix of displacement approximations, one has a symbolic representation for the discretized unknown fields, whose matrix \mathbf{N}^e has dimensions $7 \times 7(Nne + npar)$, with $npar$ equal to the number of enrichment parameters of the element.

The electric potential approximation in the coplanar directions (x, y) , in any position within a piezoelectric ply k , according to the GFEM methodology, is built with the same PoU functions, $\mathbb{N}_{no}^e(x, y)$, used to approximate the mechanical displacement fields. The approximation $\tilde{\varphi}^{k^e}(\mathbf{x}, t)$ is expressed by

$$\tilde{\varphi}^{k^e}(\mathbf{x}, t) = \sum_{no=1}^{Nne} \mathbb{N}_{no}^e(x, y) \left(\varphi_{no}^k(z, t) + \sum_{j=1}^{nf(\varphi_{no}^k)} \varphi_{no}^{kj}(z, t) f_{\varphi_{no}^k}^j(x, y) \right) \tag{32}$$

Substituting (28) into (32) one obtains

$$\begin{aligned} \tilde{\varphi}^{k^e}(\mathbf{x}, t) = & \sum_{no=1}^{Nne} \mathbb{N}_{no}^e(x, y) \left\{ \begin{bmatrix} \varphi_{no}^{k-1}(t) & \zeta_{k-1} + \varphi_{no}^k(t) & \zeta_k \end{bmatrix} \right. \\ & \left. + \sum_{j=1}^{nf(\varphi_{no}^k)} \begin{bmatrix} \varphi_{no}^{k-1^j}(t) & \zeta_{k-1} + \varphi_{no}^{k^j}(t) & \zeta_k \end{bmatrix} f_{\varphi_{no}^k}^j(x, y) \right\} \end{aligned} \quad (33)$$

All degrees of freedom involving electric and mechanical unknowns are grouped in a vector of nodal parameters for an element e , associated with each node no

$$\begin{aligned} \mathbb{U}_{no}^{eT} = & \left\{ \dots u_{no}^0, u_{no}^{0^1}, \dots, u_{no}^{0^{nf(u_{no}^0)}}, v_{no}^0, v_{no}^{0^1}, \dots, v_{no}^{0^{nf(v_{no}^0)}}, \right. \\ & w_{no}^0, w_{no}^{0^1}, \dots, w_{no}^{0^{nf(w_{no}^0)}}, \dots, \psi_{3y_{no}}, \psi_{3y_{no}}^1, \dots, \psi_{3y_{no}}^{nf(\psi_{3y_{no}})}, \\ & \varphi_{no}^1, \varphi_{no}^{1^1}, \dots, \varphi_{no}^{1^{nf(\varphi_{no}^1)}}, \varphi_{no}^2, \varphi_{no}^{2^1}, \dots, \varphi_{no}^{2^{nf(\varphi_{no}^2)}}, \dots \\ & \left. \dots, \varphi_{no}^N, \varphi_{no}^{N^1}, \dots, \varphi_{no}^{N^{nf(\varphi_{no}^N)}} \dots \right\} \end{aligned} \quad (34)$$

The extensional, flexural and warp strains can be grouped in a vector $\boldsymbol{\varepsilon}_{mf}$ such that

$$\boldsymbol{\varepsilon}_{mf} = \begin{Bmatrix} \boldsymbol{\varepsilon}^0 \\ \boldsymbol{\kappa}_1 \\ \boldsymbol{\kappa}_3 \end{Bmatrix} \quad (35)$$

In this way, the approximation of the coplanar strains over an arbitrary element e is accomplished by substituting (31) into (24). Thus we obtain

$$\begin{aligned} \tilde{\boldsymbol{\varepsilon}}(\mathbf{x}, t)^e = & \sum_{no=1}^{Nne} \mathbb{B}_{mf_{no}}^e(x, y) \mathbb{U}_{no}^e(t) \\ = & \mathbf{B}_{mf}^e \mathbf{U}^e \end{aligned} \quad (36)$$

This provides the *in-plane strains approximation matrix*, \mathbf{B}_{mf}^e , of dimensions $9 \times 7(Nne + npar)$.

Similarly, the transverse shear strains can be grouped as

$$\boldsymbol{\gamma}_c = \begin{Bmatrix} \gamma^0 \\ 3\kappa_2 \end{Bmatrix} \quad (37)$$

These strains are approximated over an element e by substituting (31) into (26) as follows

$$\begin{aligned} \tilde{\boldsymbol{\gamma}}_c(\mathbf{x}, t)^e &= \sum_{no=1}^{Nne} \mathbb{B}_{c_{no}}^e(x, y) \mathbb{U}_{no}^e(t) \\ &= \mathbf{B}_c^e \mathbf{U}^e \end{aligned} \quad (38)$$

leading to the *transverse shear approximation matrix*, \mathbf{B}_c^e , of dimensions $4 \times 7(Nne + npar)$.

The electric field vector $\mathbf{E}(\mathbf{x}, t)$ is defined as the negative gradient of the electric potential function, such that

$$\mathbf{E}(\mathbf{x}, t) = -\nabla \varphi(\mathbf{x}, t) = \begin{Bmatrix} E_x \\ E_y \\ E_z \end{Bmatrix} = \begin{Bmatrix} -\frac{\partial \varphi(\mathbf{x}, t)}{\partial x} \\ -\frac{\partial \varphi(\mathbf{x}, t)}{\partial y} \\ -\frac{\partial \varphi(\mathbf{x}, t)}{\partial z} \end{Bmatrix} \quad (39)$$

Then, using the definition of $\tilde{\varphi}(\mathbf{x}, t)^{ke}$ in (33), it is possible to express the electric field approximation over an element e , within a piezoelectric ply k , by

$$\tilde{\mathbf{E}}(\mathbf{x}, t)^{k^e} = - \sum_{no=1}^{Nne} \left\{ \begin{array}{l} \frac{\partial}{\partial x} \left\{ \mathbb{N}_{no}^e(x, y) \left[\varphi_{no}^{k-1}(t) \zeta_{k-1} \right. \right. \\ \quad \left. \left. + \varphi_{no}^k(t) \zeta_k \right] \right\} \\ \frac{\partial}{\partial y} \left\{ \mathbb{N}_{no}^e(x, y) \left[\varphi_{no}^{k-1}(t) \zeta_{k-1} \right. \right. \\ \quad \left. \left. + \varphi_{no}^k(t) \zeta_k \right] \right\} \\ \frac{\partial}{\partial z} \left\{ \mathbb{N}_{no}^e(x, y) \left[\varphi_{no}^{k-1}(t) \zeta_{k-1} \right. \right. \\ \quad \left. \left. + \varphi_{no}^k(t) \zeta_k \right] \right\} \end{array} \right\} \quad (40)$$

Finally, the electric field vector within a piezoelectric ply k can be approximated in the form

$$\begin{aligned} \tilde{\mathbf{E}}(\mathbf{x}, t)^{k^e} &= - \sum_{no=1}^{Nne} \mathbb{B}_{no}^{k^e} \mathbb{U}_{no}^e \\ &= -\mathbf{B}^{k^e} \mathbf{U}^e \end{aligned} \quad (41)$$

This equation provides the *electric field approximation matrix* within a piezoelectric ply k , \mathbf{B}^{k^e} , of dimensions $3 \times 7(Nne + npar)$.

Implementing each portion of the Hamilton's Principle functional and inserting the variable discretizations we obtain the expression for the element contributions as follows. From the variation in the potential energy it is possible to identify the purely mechanical stiffness, composed of a membrane-bending matrix, \mathbf{K}_{mf}^e , and transverse shear \mathbf{K}_c^e matrix, whose integrations over the midplane domain lead to the following representations

$$\mathbf{K}_{mf}^e = \int_{\Omega_e} \mathbf{B}_{mf}^{eT} \begin{bmatrix} \mathbf{A} & \mathbf{B} & \mathbf{L} \\ \mathbf{B} & \mathbf{D} & \mathbf{F} \\ \mathbf{L} & \mathbf{F} & \mathbf{H} \end{bmatrix} \mathbf{B}_{mf}^e d\Omega_e \quad (42)$$

$$\mathbf{K}_c^e = \int_{\Omega_e} \mathbf{B}_c^{eT} \begin{bmatrix} \mathbf{A}_c & \mathbf{D}_c \\ \mathbf{D}_c & \mathbf{F}_c \end{bmatrix} \mathbf{B}_c^e d\Omega_e \quad (43)$$

The sub-matrices \mathbf{A} , \mathbf{B} , \mathbf{D} , \mathbf{F} , \mathbf{H} and \mathbf{L} are components of the *purely mechanical constitutive matrix of membrane and bending of the laminate*, of dimensions 9×9 , and the sub-matrices \mathbf{A}_c , \mathbf{D}_c , \mathbf{F}_c , are the components of the *purely mechanical constitutive matrix of transverse shear of the laminate*. These matrix components are obtained by integrating across the thickness in the following way

$$\begin{aligned} \{A_{ij}, B_{ij}, D_{ij}, L_{ij}, F_{ij}, H_{ij}\} &= \\ &= \sum_{k=1}^N \int_{z_{k-1}}^{z_k} C_{ij}^k \{1, z, z^2, z^3, z^4, z^6\} dz, \quad i, j = 1, 2, 6. \end{aligned} \quad (44)$$

$$\begin{aligned} \{A_{c_{ij}}, D_{c_{ij}}, F_{c_{ij}}\} &= \\ &= \sum_{k=1}^N \int_{z_{k-1}}^{z_k} C_{ij}^k \{1, z^2, z^4\} dz, \quad i, j = 4, 5. \end{aligned} \quad (45)$$

At this point it is convenient to decompose the electric field in each piezoelectric layer k into a constant and a linearly varying part across its thickness, in the form

$$\begin{aligned} \tilde{\mathbf{E}}^{ke}(\mathbf{x}, t) &= - \sum_{no=1}^{Nne} \left\{ \mathbb{E}_{no}^{0k} + z \mathbb{E}_{no}^{1k} \right\} \\ &= - \left\{ \mathbf{E}^{0k} + z \mathbf{E}^{1k} \right\} \end{aligned} \quad (46)$$

Similarly to the forms used for the deformation equations, (35) or (37), it is useful to group the electric field \mathbf{E}^{0k} and \mathbf{E}^{1k} , in definition (46), in the following way

$$\tilde{\mathbf{E}}^{ke} = - \begin{Bmatrix} \mathbf{E}^{0k} \\ \mathbf{E}^{1k} \end{Bmatrix} \quad (47)$$

From the expression of the variation of strain energy, it is also possible to identify the coupled mechanical-electrical stiffness, composed of a membrane-bending coupled stiffness part $\mathbf{K}_{mf-\varphi}^e$ and a transverse shear coupled stiffness $\mathbf{K}_{c-\varphi}^e$, whose integration on the in-plane domain results in

$$\mathbf{K}_{mf-\varphi}^e = \int_{\Omega_e} \mathbf{B}_{mf}^{eT} \begin{bmatrix} \mathbf{O} & \mathbf{P} \\ \mathbf{P} & \mathbf{Q} \\ \mathbf{R} & \mathbf{S} \end{bmatrix}^{lam} \begin{bmatrix} \mathbf{E}^{1e} \\ \vdots \\ \mathbf{E}^{n_{piez}e} \end{bmatrix} d\Omega_e \quad (48)$$

$$\mathbf{K}_{c-\varphi}^e = \int_{\Omega_e} \mathbf{B}_c^{eT} \begin{bmatrix} \mathbf{T} & \mathbf{U} \\ \mathbf{V} & \mathbf{W} \end{bmatrix}^{lam} \begin{bmatrix} \mathbf{E}^{1e} \\ \vdots \\ \mathbf{E}^{n_{piez}e} \end{bmatrix} d\Omega_e \quad (49)$$

The sub-matrices $\mathbf{O}^k, \mathbf{P}^k, \mathbf{Q}^k, \mathbf{R}^k$ and \mathbf{S}^k are independents for each piezoelectric layer k , defining a *mechanically-electrically coupled constitutive matrix for membrane-bending of the laminate*, of order $9 \times 6n_{piez}$, and the sub-matrices $\mathbf{T}^k, \mathbf{U}^k, \mathbf{V}^k$ and \mathbf{W}^k , defining a *mechanical-electrically coupled constitutive matrix for shear bending of the laminate*, of order $4 \times 6n_{piez}$. Their components are given by

$$\begin{aligned} \{O_{ij}^k, P_{ij}^k, Q_{ij}^k, R_{ij}^k, S_{ij}^k\} &= \\ &= \int_{z_{k-1}}^{z_k} e_{ij}^k \{1, z, z^2, z^3, z^4\} dz, \quad i, j = 1, 2, 6. \end{aligned} \quad (50)$$

$$\begin{aligned} \{T_{ij}^k, U_{ij}^k, V_{ij}^k, W_{ij}^k\} &= \\ &= \int_{z_{k-1}}^{z_k} e_{ij}^k \{1, z, z^2, z^3\} dz, \quad i, j = 4, 5. \end{aligned} \quad (51)$$

The *electrically-mechanically coupled stiffness matrix*, $\mathbf{K}_{\varphi u}^e$, is obtained by a similar procedure to that used for the *mechanically-electrically coupled stiffness matrix*, $\mathbf{K}_{u\varphi}^e$. It should be noted that $\mathbf{K}_{\varphi u}^e = \mathbf{K}_{u\varphi}^{e^T}$.

Finally, the *purely electrical stiffness matrix* $\mathbf{K}_{\varphi\varphi}^e$ can be obtained by in-plane integration by

$$[\mathbf{K}_{\varphi\varphi}^e] = \int_{\Omega_e} \begin{bmatrix} \mathbf{E}^{1e} \\ \vdots \\ \mathbf{E}^{n_{piez}e} \end{bmatrix}^T \begin{bmatrix} \mathbf{X} & \mathbf{Y} \\ \mathbf{Y} & \mathbf{Z} \end{bmatrix}^{lam} \begin{bmatrix} \mathbf{E}^{1e} \\ \vdots \\ \mathbf{E}^{n_{piez}e} \end{bmatrix} d\Omega_e \quad (52)$$

The *purely electrical constitutive matrix of the laminate* is of order $6n_{piez} \times 6n_{piez}$ and it is formed by sub-matrices \mathbf{X}^k , \mathbf{Y}^k and \mathbf{Z}^k , whose components are given by

$$\begin{aligned} \{X_{ij}, Y_{ij}, Z_{ij}\} &= \\ &= \int_{z_{k-1}}^{z_k} \chi_{ij}^k \{1, z, z^2\} dz, \quad i, j = 1, 2, 3. \end{aligned} \quad (53)$$

The total element stiffness matrix is obtained adding all contributions

$$\mathbf{K}^e = \mathbf{K}_{uu}^e + \mathbf{K}_{u\varphi}^e + \mathbf{K}_{\varphi u}^e - \mathbf{K}_{\varphi\varphi}^e \quad (54)$$

The *element inertia matrix* \mathbf{M}^e is obtained by inserting the mechanical displacement approximation into the variation in the kinetic energy and performing integration on the element midplane domain Ω_e . This results in

$$\mathbf{M}^e = \int_{\Omega_e} \mathbf{N}^{e^T} \begin{bmatrix} \mathbf{P}_0 & \mathbf{P}_1 & \mathbf{P}_3 \\ \mathbf{P}_1 & \mathbf{P}_2 & \mathbf{P}_4 \\ \mathbf{P}_3 & \mathbf{P}_4 & \mathbf{P}_6 \end{bmatrix} \mathbf{N}^e d\Omega_e \quad (55)$$

where $\mathbf{P}_0 = \rho_0 I_{3x3}$, $\mathbf{P}_1 = \rho_1 I_{3x2}$, $\mathbf{P}_2 = \rho_2 I_{2x2}$, $\mathbf{P}_3 = \rho_3 I_{3x2}$, $\mathbf{P}_4 = \rho_4 I_{2x2}$ and $\mathbf{P}_6 = \rho_6 I_{2x2}$. The $I_{3x2} = \delta_{ij}$, $1 \leq i \leq 3$, $1 \leq j \leq 2$ and the $I_{2x2} = \delta_{ij}$, $1 \leq i \leq 2$, $1 \leq j \leq 2$. The generalized masses are defined by:

$$\begin{aligned} \{\rho_0, \rho_1, \rho_2, \rho_3, \rho_4, \rho_6\} &= \\ &= \sum_{k=1}^N \int_{z_{k-1}}^{z_k} \rho_k \{1, z, z^2, z^3, z^4, z^6\} dz \end{aligned} \quad (56)$$

where ρ_k is an equivalent mass per unit area of the layer k .

Similarly, the *vectors of equivalent nodal forces* are obtained from the variation in the external work, such that

$$\begin{aligned} \mathbf{F}^{e^V} &= \int_{\Omega_e} \mathbf{N}_{uu}^{e^T} \mathbf{N}^{f^e} F^V d\Omega_e \\ \mathbf{F}^{e^S} &= \int_{\Omega_e} \mathbf{N}_{uu}^{e^T} \mathbf{N}^{f^e} F^S d\Omega_e \\ \mathbf{F}^{e^P} &= \mathbf{N}_{uu}^{e^T} F^P \\ \mathbf{F}^{e^Q} &= \int_{\Omega_e} \mathbf{N}_{\varphi\varphi}^{e^T} \mathbf{N}^{q^e} Q^S d\Omega_e \end{aligned} \quad (57)$$

\mathbf{N}_{uu}^e and $\mathbf{N}_{\varphi\varphi}^e$ are approximation arrays for the mechanical and electrical unknowns, respectively. All the contributions are assembled into the element nodal force vector $\mathbf{F}^e(t)$.

The semi-discrete algebraic equations of motion for the element are

$$\mathbf{M}^e \ddot{\mathbf{U}}^e(t) + \mathbf{K}^e \mathbf{U}^e(t) = \mathbf{F}^e(t) \quad (58)$$

For the particular case of a quasi-static problem, the system becomes

$$\mathbf{K}^e \mathbf{U}^e = \mathbf{F}^e(t) \quad (59)$$

It is known that, even after the correct imposition of essential boundary conditions, the stiffness matrix shows a very high condition number, or becomes singular. This linear dependence between the system equations occurs because the PoU and the enrichment functions are both polynomials [27]. The algebraic solution must be obtained using a procedure suitable for positive-semi-definite matrices. The present work utilizes the iterative K- ϵ method of Babuška [28].

5. Strong formulation for the problem

The equilibrium equations, for the piezoelectric plate model used here, in terms of generalized forces, are

$$\begin{aligned} \frac{\partial N_x}{\partial x} + \frac{\partial N_{xy}}{\partial y} + \bar{q}_x &= f_x \\ \frac{\partial N_{xy}}{\partial x} + \frac{\partial N_y}{\partial y} + \bar{q}_y &= f_y \\ \frac{\partial Q_x}{\partial x} + \frac{\partial Q_y}{\partial y} + \bar{q}_z &= f_z \\ \frac{\partial M_x}{\partial x} + \frac{\partial M_{xy}}{\partial y} - Q_x + \bar{m}_y &= f_{mx} \end{aligned}$$

$$\begin{aligned}
\frac{\partial M_{xy}}{\partial x} + \frac{\partial M_y}{\partial y} - Q_y - \bar{m}_x &= f_{my} \\
\frac{\partial M_{3x}}{\partial x} + \frac{\partial M_{3xy}}{\partial y} - 3Q_{2x} + \bar{m}_{3y} &= f_{3mx} \\
\frac{\partial M_{3xy}}{\partial x} + \frac{\partial M_{3y}}{\partial y} - 3Q_{2y} - \bar{m}_{3x} &= f_{3my} \\
\frac{\partial L_x^{(k)}}{\partial x} + \frac{\partial L_y^{(k)}}{\partial y} - J_k + \bar{q}_{ek} &= 0
\end{aligned} \tag{60}$$

The generalized resultant internal forces are defined as

$$\{\mathbf{N}, \mathbf{M}, \mathbf{M}_3\} = \sum_{k=1}^N \int_{z_{k-1}}^{z_k} \boldsymbol{\sigma}^{(k)} \{1, z, z^3\} dz \tag{61}$$

$$\{\mathbf{Q}, \mathbf{Q}_2\} = \sum_{k=1}^N \int_{z_{k-1}}^{z_k} \boldsymbol{\tau}^{(k)} \{1, z^2\} dz \tag{62}$$

$$\mathbf{L}^{(k)} = \begin{Bmatrix} L_x \\ L_y \end{Bmatrix}^{(k)} = \int_{z_{k-1}}^{z_k} \left(\frac{z - z_k}{h_k} \right) \begin{Bmatrix} D_x \\ D_y \end{Bmatrix}^{(k)} dz \tag{63}$$

$$J_k = \int_{z_{k-1}}^{z_k} \frac{D_z^{(k)}}{h_k} dz \tag{64}$$

where $\mathbf{N} = \{N_x \ N_y \ N_{xy}\}^T$, $\mathbf{M} = \{M_x \ M_y \ M_{xy}\}^T$ and $\mathbf{M}_3 = \{M_{3x} \ M_{3y} \ M_{3xy}\}^T$ are in-plane stress resultants, whereas $\mathbf{Q} = \{Q_y \ Q_x\}^T$ and $\mathbf{Q}_2 = \{Q_{2y} \ Q_{2x}\}^T$ are transverse shear stress resultants, $\boldsymbol{\sigma} = \{\sigma_x \ \sigma_y \ \tau_{xy}\}^T$ and $\boldsymbol{\tau} = \{\tau_{yz} \ \tau_{xz}\}^T$. It is important to note that both $\mathbf{L}^{(k)}$, the in-plane electrical displacement resultant, and J_k , the transversal electrical displacement resultant, are defined for each piezoelectric layer.

In the derivation of the virtual work done by the external forces, the body is considered to be subjected to distributed forces on the upper surface $\{\bar{q}_{sx} \ \bar{q}_{sy} \ \bar{q}_{sz}\}$, on the lower surface $\{\bar{q}_{ix} \ \bar{q}_{iy} \ \bar{q}_{iz}\}$ and on the boundary $\{\bar{T}_n \ \bar{T}_{ns} \ \bar{T}_{nz}\}$. \bar{T}_n , \bar{T}_{ns} and \bar{T}_{nz} are the normal, in-plane and transverse shear forces per unity area, respectively. It

is assumed the volumetric free charge is zero, that is, $\bar{Q}_e = 0$, since the piezoelectric material is dielectric and does not contain free electric charge. Also, in this work the application of free electric charge on the surface, denoted by \bar{q}_{ek} , is assumed only on the lower surface of a piezoelectric layer k . The upper surface of each layer is assumed to be free of charge. Additionally, it is important to note that $\delta\varphi$ is assumed to be null on the upper surface of each piezoelectric layer.

In (60) the following generalized external forces on the bi-dimensional domain are defined

$$\begin{aligned} \begin{Bmatrix} \bar{q}_x \\ \bar{q}_y \\ \bar{q}_z \end{Bmatrix} &= \begin{Bmatrix} \bar{q}_{sx} + \bar{q}_{ix} \\ \bar{q}_{sy} + \bar{q}_{iy} \\ \bar{q}_{sz} + \bar{q}_{iz} \end{Bmatrix} + \int_{-h/2}^{h/2} \begin{Bmatrix} F_x \\ F_y \\ F_z \end{Bmatrix} dz \\ \begin{Bmatrix} \bar{m}_x \\ \bar{m}_y \end{Bmatrix} &= \frac{h}{2} \begin{Bmatrix} \bar{q}_{iy} - \bar{q}_{sy} \\ \bar{q}_{sx} - \bar{q}_{ix} \end{Bmatrix} + \int_{-h/2}^{h/2} z \begin{Bmatrix} -F_y \\ F_x \end{Bmatrix} dz \\ \begin{Bmatrix} \bar{m}_{3x} \\ \bar{m}_{3y} \end{Bmatrix} &= \frac{h^3}{8} \begin{Bmatrix} \bar{q}_{iy} - \bar{q}_{sy} \\ \bar{q}_{sx} - \bar{q}_{ix} \end{Bmatrix} + \int_{-h/2}^{h/2} z^3 \begin{Bmatrix} -F_y \\ F_x \end{Bmatrix} dz \end{aligned} \quad (65)$$

Moreover, the generalized external forces applied on the boundary are

$$\begin{Bmatrix} \bar{N}_n & \bar{M}_n \\ \bar{N}_{ns} & \bar{M}_{ns} \\ \bar{Q}_n & \bar{M}_{3n} \\ & \bar{M}_{3ns} \end{Bmatrix} = \int_{-h/2}^{h/2} \begin{Bmatrix} \bar{T}_n & z\bar{T}_n \\ \bar{T}_{ns} & z\bar{T}_{ns} \\ \bar{T}_{nz} & z^3\bar{T}_n \\ & z^3\bar{T}_{ns} \end{Bmatrix} dz \quad (66)$$

and the generalized inertial forces are

$$\begin{aligned}
f_x &= \ddot{u}^0 \rho_0 + \ddot{\psi}_x \rho_1 + \ddot{\psi}_{3x} \rho_3, \\
f_y &= \ddot{v}^0 \rho_0 + \ddot{\psi}_y \rho_1 + \ddot{\psi}_{3y} \rho_3, \\
f_z &= \ddot{w}^0 \rho_0, \\
f_{mx} &= \ddot{u}^0 \rho_1 + \ddot{\psi}_x \rho_2 + \ddot{\psi}_{3x} \rho_4, \\
f_{my} &= \ddot{v}^0 \rho_1 + \ddot{\psi}_y \rho_2 + \ddot{\psi}_{3y} \rho_4, \\
f_{3mx} &= \ddot{u}^0 \rho_3 + \ddot{\psi}_x \rho_4 + \ddot{\psi}_{3x} \rho_6, \\
f_{3my} &= \ddot{v}^0 \rho_3 + \ddot{\psi}_y \rho_4 + \ddot{\psi}_{3y} \rho_6
\end{aligned} \tag{67}$$

where the generalized mass moments are defined as

$$\rho_j = \sum_{k=1}^N \int_{z_{k-1}}^{z_k} \rho^{(k)} z^j dz, \quad j = 0, 1, 2, 3, 4, 6. \tag{68}$$

The following variational consistent boundary conditions are also obtained

$$\begin{aligned}
N_n &= \overline{N}_n & M_n &= \overline{M}_n & M_{3n} &= \overline{M}_{3n} \\
N_{ns} &= \overline{N}_{ns} & M_{ns} &= \overline{M}_{ns} & M_{3ns} &= \overline{M}_{3ns} \\
Q_n &= \overline{Q}_n
\end{aligned} \tag{69}$$

on Γ_σ of the reference surface and $L_n^{(k)} = 0$ on $\Gamma_q^{(k)}$ of the lower surface of each piezoelectric layer k . If there is a free electric charge distributed on the piezoelectric surface, one has the boundary condition $L_n^{(k)} = \overline{L}_m^{(k)}$.

6. Numerical results

The present GFEM formulation for piezoelectric laminated composite plates was incorporated into a finite element code written with FORTRAN 90 from which numerical solutions for some study cases were obtained. The verification was conducted

by comparison with the analytical solutions for the proposed problems, obtained from the formulation shown in Section 5 using the Navier's Method. Next, the results for convergence in a global measure of the relative error in energy norm and a pointwise assessment of stresses as well as of electric field are displayed. This assessment is carried out through the static analysis of square composite laminated plates, thick and thin, with continuous piezoelectric layers, in active and sensor modes.

6.1. Case 1 - Static bending analysis of a plate with piezoelectric sensors

The first problem consists of a thick square laminated composite plate with continuous piezoelectric sensors bonded on its faces. The plate dimensions are 1000 mm \times 1000 mm and a thickness of 100 mm, and the plate is simply supported at all boundaries and subjected to a uniformly distributed mechanical force. The piezoelectric layers have only the bottom surface under the free potential condition, i.e., the top surface of the piezoelectric layers are grounded, with null potential imposed. The stacking sequence is [0/0/90/90/0/0], as shown in Figure 1(a). The piezoelectric layers have 10 mm of thickness each and the host laminate has layers with thicknesses of 26.66 mm, 13.33 mm, 13.33 mm, 26.66 mm, respectively.

The material properties for the substrate layers are

$$\begin{aligned} E_1 &= 172.25 \text{ GPa} & E_2 = E_3 &= 6.89 \text{ GPa} \\ G_{12} = G_{13} &= 3.45 \text{ GPa} & G_{23} &= 2.75 \text{ GPa} \\ \nu_{23} &= 0.25 & \nu_{12} = \nu_{13} &= 0.25 \end{aligned}$$

and the material properties for PZT-4 are

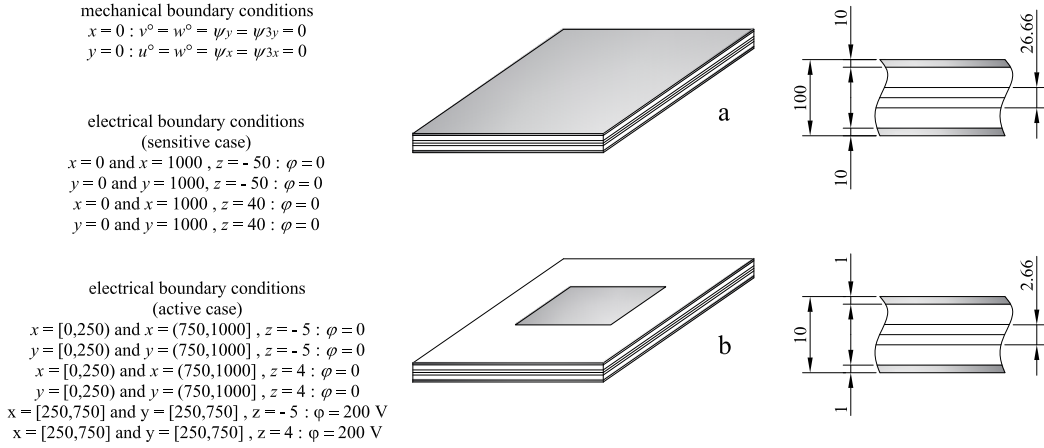


Figure 1: Two laminated composite plates, one thick (a) and the other thin (b), for the passive and active cases, respectively. The mechanical and electrical boundary conditions are shown, as well as the thickness of the layers. All dimensions are in millimeters.

$$\begin{array}{ll}
E_1 = E_2 = 94.95 \text{ GPa} & E_3 = 81.89 \text{ GPa} \\
G_{12} = 35.90 \text{ GPa} & G_{13} = G_{23} = 25.40 \text{ GPa} \\
\nu_{12} = 0.32 & \nu_{13} = \nu_{23} = 0.38 \\
e_{15} = e_{24} = 9.20 \text{ C/m}^2 & e_{31} = e_{32} = -2.10 \text{ C/m}^2 \\
e_{33} = 9.50 \text{ C/m}^2 & \\
\chi_{11} = \chi_{22} = 4.07 \times 10^{-9} \text{ F/m} & \chi_{33} = 2.08 \times 10^{-9} \text{ F/m}
\end{array}$$

Three regular meshes were considered, as shown in Figure 2, over which isotropic enrichment up to third polynomial degree was applied, for all generalized unknowns.

In sequence, the meshes were modified by a distortion of the elements, as shown in Figure 3. For the mesh with the poorest h -refinement, the pattern of distortion is shown by the dimensions and corresponds to the mesh shown in Figure 3(a). The

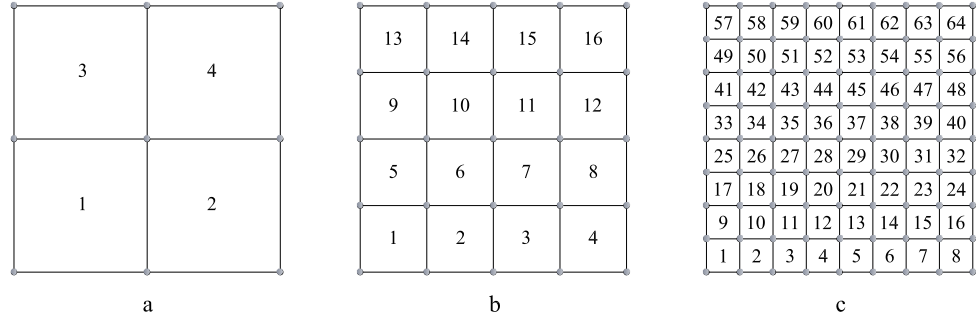


Figure 2: Three regular meshes of generalized finite elements. All meshes are used for the passive case but only the last two, (b) and (c), are used for the active case.

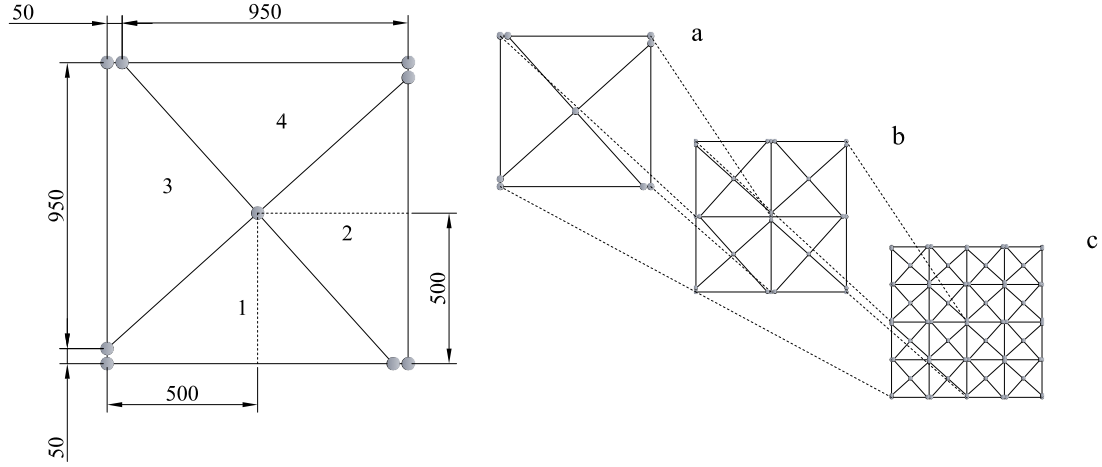


Figure 3: Three distorted meshes used for the passive case. All dimensions are in millimeters. The dimensional proportions are respected in the enriched h -refinements.

same pattern was used, respecting the proportions, and it was repeated four and sixteen times for the meshes (b) and (c), respectively, both in Figure 3.

As a global measure of convergence, the relative error in energy norm was considered, following (70), evaluated from the numerical energy of deformation, E , and the analytical energy of deformation, E_{ref} .

$$Error_{rel} = \sqrt{\frac{E - E_{ref}}{E_{ref}}} \quad (70)$$

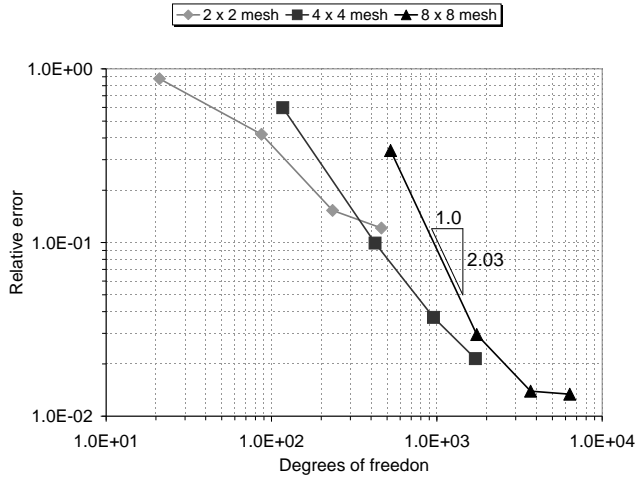


Figure 4: Relative error in energy norm considering p -refinement for different regular meshes.

Figure 4 shows the convergence rates for the p -enrichment over the fixed regular meshes. Figure 5 shows the convergence rates when h -refinement is applied for different polynomial degrees. It can be observed that there is a tendency to form envelopes which exhibit a rate of convergence for p -refinement which is approximately twice that for h -refinement, as it to be expected.

The convergence rates for p -enrichment on distorted meshes are plotted in Figure 6. Since the enrichment is built with functions defined in global coordinates, even with distorted meshes the characteristic rate of convergence for p -refinement is practically maintained.

Nevertheless, it should be noted that as the number of degrees of freedom becomes very large the ill-conditioning of the stiffness matrix does not allow effective error reductions. In this case, this is occurring due to the linear dependence between the PoU and enrichment functions and also because the problem under analysis has many physical unknowns and mainly because the material properties have very different magnitudes.

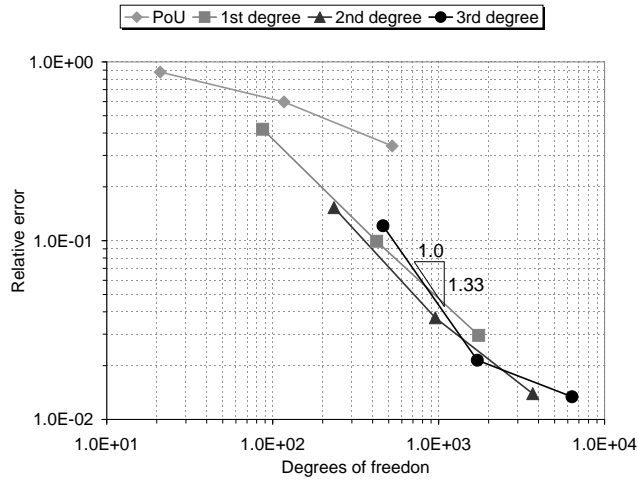


Figure 5: Relative error in energy norm considering h -refinement with four polynomial degrees.

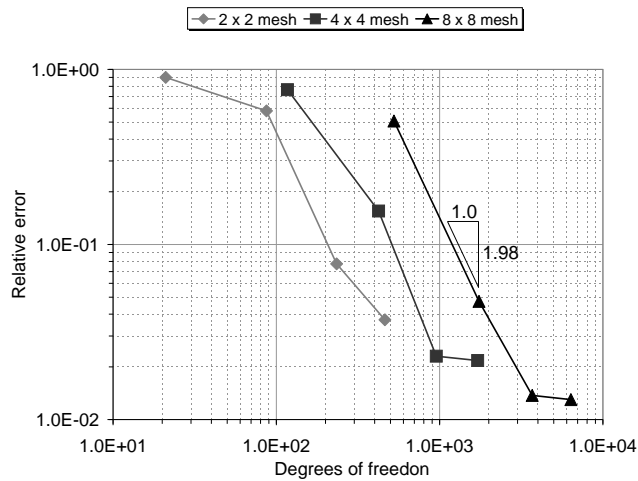


Figure 6: Relative error in energy norm considering p -refinement for different distorted meshes.

The quality of the numerical solution may be showed by pointwise evaluation of stresses and electric field. For this reason, the selected points for stress measurements were defined as displayed in Figure 7. These points correspond to the 3×3 Gauss quadrature rule for the elements 1, 2, 5 and 6 of the mesh (b) in Figure 2. Their global coordinates are listed in Table 1.

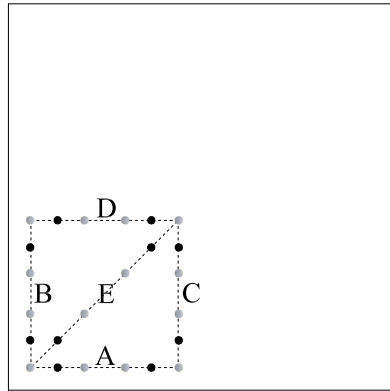


Figure 7: Lines A to E, over which the points where the stresses and electric field are calculated are located.

For the stress computation the following nondimensionalized stress definitions, S_{xx} and S_{yz} , were considered

$$S_{xx}^k = \sigma_{xx}^k \frac{h^2}{b^2 q_0} \frac{E_1^k}{E_{1comp}} \quad (71)$$

$$S_{yz}^k = \tau_{yz}^k \frac{h}{b q_0}$$

where b is the plate dimension, h is the total thickness and q_0 is the load value. The parameter E_1^k/E_{1comp} , where $comp$ stands for the base materials (layers 2 to 5)

Table 1: Global coordinates of the points selected for the stress calculations.

line	coordinates	1	2	3	4	5	6
A	x	28.175	125.000	221.825	278.175	375.000	471.825
	y	28.175	28.175	28.175	28.175	28.175	28.175
C	x	471.825	471.825	471.825	471.825	471.825	471.825
	y	28.175	125.000	221.825	278.175	375.000	471.825
E	x	28.175	125.000	221.825	278.175	375.000	471.825
	y	28.175	125.000	221.825	278.175	375.000	471.825

and k stands for a given layer, is used to allow a better comparison between the stress values in different materials. This scaling is not used for the transverse shear stress because it is piecewise continuous from the integration of the local equilibrium differential equations.

Figure 8 shows the nondimensionalized in-plane stress S_{xx} across the plate thickness, computed at the points along line C of Figure 7, for the mesh (b) in Figure 2. The PoU can not approximate the stress and for the first degree enrichment the computed values are very close the stresses provided by the analytical solution. It is important to note in Figure 8(a) that the first degree enrichment is not able to predict the stress in the outermost layers, which is a consequence of the way in which the boundary conditions are imposed.

Figure 9 shows the distribution of the nondimensionalized transverse shear stresses S_{yz} evaluated through integration of the local equilibrium differential equations, at the points over line A in Figure 7. In relation to 9(a), (b) and (c), for the points in the element closest to the plate corner, the approximation functions are poorer than

at the inner elements due to the essential boundary conditions. But the third-degree enrichment allows a better approximation of the analytical solution for all points, even that closest to the middle point of the boundary.

Figure 10 shows the electric fields computed in the piezoelectric sensors, at the points over line E of Figure 7.

6.2. Case 2 - Static bending analysis of a plate with piezoelectric actuators

A second problem was considered in order to verify the applicability of the present formulation in the analysis of thin plates and its performance for the active case.

In order to identify possible singularities, an electric potential of 200 V was considered, applied to the actuators only on a region at the plate center, as shown in Figure 1(b), negative on the top and positive on the bottom piezoelectric layer. Since the plate is thin, these electrical boundary conditions lead to a solution whose higher-order generalized rotation only diverges from zero over the boundary of the region where the potentials are applied, with a sharp gradient, as can be seen in Figure 11. The first one thousand terms were considered in the computation of the solution using trigonometric series.

The material properties for the substrate layer are

$$E_1 = 132.38 \text{ GPa} \quad E_2 = E_3 = 10.76 \text{ GPa}$$

$$G_{12} = 3.61 \text{ GPa} \quad G_{13} = G_{23} = 5.65 \text{ GPa}$$

$$\nu_{12} = \nu_{13} = 0.24 \quad \nu_{23} = 0.49$$

and the material properties for PVDF are

$$\begin{aligned}
E_1 &= E_2 = E_3 = 62.97 \text{ GPa} \\
G_{12} &= G_{13} = G_{23} = 24.20 \text{ GPa} & \nu_{12} &= \nu_{13} = \nu_{23} = 0.30 \\
e_{15} &= e_{24} = 14.13 \text{ C/m}^2 & e_{31} &= e_{32} = 18.41 \text{ C/m}^2 \\
e_{33} &= 12.51 \text{ C/m}^2 \\
\chi_{11} &= \chi_{22} = \chi_{33} = 15.30 \times 10^{-7} \text{ F/m}
\end{aligned}$$

In this case, two meshes were considered, as shown in Figures 2(b) and 2(c), on which enrichment was applied up to the third-degree polynomial.

All the mechanical stresses were evaluated at the points over line E shown in Figure 7, but this time only at the grey points, since the black points lie on the interelement boundaries of mesh (c), in Figure 6, and thus one avoids auxiliary procedures to regularize the stress fields.

In this case, the stress results shown were obtained using the following nondimensional form

$$\begin{aligned}
S_{xx}^k &= \sigma_{xx}^k \frac{b^2}{h^2 E_{1_{piez}}} \frac{E_1^k}{E_{1_{comp}}} \\
S_{yz}^k &= \tau_{yz}^k \frac{b}{h E_{1_{piez}}}
\end{aligned} \tag{72}$$

where b is the plate dimension, h is the total thickness, $piez$ stands for piezoelectric material and the parameter $E_1^k/E_{1_{comp}}$ is also used to scale the values. Such scaling is not applied to the transverse shear stress because it is piecewise continuous.

In Figure 12 it can be noted that the approximated nondimensionalized in-plane stress S_{xx} is more accurately reproduced within the region where the potential is applied than in the complementary portion of the domain. Since a higher polynomial degree is used in these calculations, the results shown in Figures 12(a) and (b)

indicate the need for h-refinement to improve the approximate solution. Figure 13 shows good accuracy for the in-plane shear stresses. This is not seen for the transverse shear stresses (Figure 14) because, since the plate is thin, the contribution of the higher generalized rotations in the computation of stress derivatives is very small. Also, in this problem, the transverse shear stresses are very small compared to the in-plane stresses.

Concluding remarks

The generalized finite element formulation presented here was implemented and verified by comparison with the respective analytical solution. This formulation is based on a mixed HSDT-Layerwise model for laminated composite plates with piezoelectric layers where both the active and sensory behaviors are modeled. This mixed model represents an efficient tool for modeling adaptive plate structures and the resulting requirement of only C^0 continuity allows for the implementation of triangular or quadrilateral elements. The GFEM methodology for enriching approximation subspaces is very versatile and may be easily understood as a extension to the conventional FEM formulation if a Lagrangian finite element based Partition of Unity is used. In this procedure, the enrichment degree may vary over the connected domain without loss of continuity and it is also possible to enrich only some generalized unknowns of the model. The performance on application to the static behavior of piezoelectric plates was verified and good quality approximation can be obtained

using either global error measurements or pointwise stress and potential computations. The reference results were obtained from the analytical solutions developed and computed by the authors. The p -refinement leads to results that agree very well with the reference values. The formulation is applicable to thin or thick plates without locking, since the p -refinement behaves as a classical hierarchical FEM, even though no specific strategies to deal with locking were included. For thick plates, the results are better than for thin plates because even for the transverse shear stresses, computed from the local equilibrium differential equations, the analytical values are achieved for the third-degree enrichment in both materials. The influence of the way in which the boundary conditions are enforced was also apparent from these results, because some errors occur near the boundary. Nevertheless, these errors are more noticeable in the case of the stress derivatives. The enrichment with monomials defined on global coordinates over the plane domain also improves the solutions across the thickness and makes the procedure very robust to mesh distortions. Even though the formulation was derived considering inertial effects, the results for dynamic analysis will be presented in a forthcoming paper. For tailoring toward high gradients, it is possible to use special enrichment functions to capture localized effects. Moreover, an aspect which merits attention is the ill-conditioned stiffness matrices generated due to the multiphysical phenomenon, since the material properties have very different magnitudes, and methods to deal with ill-conditioned matrices need to be developed.

Acknowledgements

D A F Torres gratefully acknowledges the financial support provided by the Brazilian government agencies CAPES (Coordenação de Aperfeiçoamento de Pessoal de Nível Superior) and CNPq (Conselho Nacional de Desenvolvimento Científico e Tecnológico) during this research.

- [1] S. Hurlebaus, L. Gaul, Smart structures dynamics: review. *Mechanical Systems and Signal Processing* 20 (2006) 255-281.
- [2] H. -J. Lee, Finite element analysis of active and sensory thermopiezoelectric composite materials (Glenn Research Center - National Aeronautics and Space Administrations) Report 210892 (2001).
- [3] H. Allik, T. J. R. Hughes, Finite element method for piezoelectric vibration. *International Journal for Numerical Methods in Engineering* 2 (1970) 151-158.
- [4] S. K. Ha, C. Keilers, F. K. Chang, Finite element analysis of composite structures containing distributed piezoceramic sensors and actuators. *AIAA Journal* 30 (1992) 772-780.
- [5] H. S. Tzou, C. I. Tseng, Distributed piezoelectric sensor/actuator design for dynamic measurement/control of distributed parameter systems: a piezoelectric finite element approach. *Journal of Sound and Vibration* 138 (1990) 17-34.
- [6] W. S. Hwang, H. C. Park, Finite element modeling of piezoelectric sensors and actuators. *AIAA Journal* 31 (1993) 930-937.
- [7] D. T. Detwiler, M. -H. H. Shen, V. B. Venkayya, Finite element analysis of laminated composite structures containing distributed piezoelectric actuators and sensors. *Finite Elements in Analysis and Design* 20 (1995) 87-100.
- [8] J. -X. Gao, Y. -P. Shen, Active control of geometrically nonlinear transient vibration of composite plates with piezoelectric actuators. *Journal of Sound and Vibration* 264 (2003) 911-928.

- [9] D. A. Saravanos, P. R. Heyliger, D. A. Hopkins, Layerwise mechanics and finite element for the dynamic analysis of piezoelectric composite plates. *International Journal of Solids and Structures* 34 (1997) 359-378.
- [10] D. A. Saravanos, Mixed laminate theory and finite element for smart piezoelectric composite shell structures. *AIAA Journal* 35 (1997) 1327-1333.
- [11] S. Cen, A. -K. Soh, Y. -Q. Long, Z. -H. Yao, A new 4-node quadrilateral FE model with variable electrical degrees of freedom for the analysis of piezoelectric laminated composite plates. *Computers and Structures* 58 (2002) 583-599.
- [12] K. M. Liew, X. Q. He, M. J. Tan, H. K. Lim, Dynamic analysis of laminated composite plates with piezoelectric sensor/actuator patches using the FSDT mesh-free method. *International Journal of Mechanical Science* 46 (2004) 411-431.
- [13] J. N. Reddy, A simple higher-order theory for laminated plates. *Journal of Applied Mechanics* 51 (1984) 745-752.
- [14] M. Levinson, An accurate simple theory of the static and dynamics of elastic plates. *Mechanics Research Communications* 7 (1980) 343-350.
- [15] K. H. Lo, R. M. Christensen, E. M. Wu, A high order theory of plate deformation 2: laminated plates. *Journal of Applied Mechanics* 44 (1977) 669-676.
- [16] J. A. Mitchell, J. N. Reddy, A refined hybrid plate theory for composite laminates with piezoelectric laminae. *International Journal of Solids and Structures* 32 (1995) 2345-2367.
- [17] J. N. Reddy, On laminated composite plates with integrated sensors and actuators. *Engineering Structures* 21 (1999) 568-593.

- [18] C. Y. K. Chee, Static shape control of laminated composite plate smart structure using piezoelectric actuators. Ph.D. dissertation, University of Sydney, 2000.
- [19] A. W. Faria, Finite element modeling of composite plates incorporating piezoelectric sensors and actuators: implementation and numerical assessment. M.Sc. dissertation. Federal University of Uberlandia (2006) (in Portuguese).
- [20] V. M. F. Correia, M. A. A. Gomes, A. Suleman, C. M. M. Soares, C. A. M. Soares, Modelling and design of adaptive composite structures. Computer Methods in Applied Mechanics and Engineering 185 (2000) 325-346.
- [21] V. Cotonni, P. Masson, F. Côté, A finite element for piezoelectric multilayered plates: combined higher-order and piecewise linear C^0 formulation. Journal of Intelligent Material Systems and Structures 17 (2006) 155-166.
- [22] J. E. S. Garo, C. M. M. Soares, C. A. M. Soares, J. N. Reddy, Analysis of laminated adaptive plate structures using layerwise finite element models. Computers and Structures 82 (2004) 1939-1959.
- [23] E. Carrera, Evaluation of layerwise mixed theories for laminated plates analysis. American Institute of Aeronautics and Astronautics Journal 36 (1998) 830-839.
- [24] R. G. Lage, C. M. M. Soares, C. A. M. Soares, J. N. Reddy, Modeling of piezo-laminated plates using layerwise mixed finite elements. Computers and Structures 82 (2004) 1849-1863.
- [25] R. G. Lage, C. M. M. Soares, C. A. M. Soares, J. N. Reddy, Layerwise partial mixed finite element analysis of magneto-electro-elastic plates. Computers and Structures 82 (2004) 1293-1301.

- [26] J. T. Oden, C. A. Duarte, O. C. Zienkiewicz, A new cloud-based hp finite element method, Computer Methods in Applied Mechanics and Engineering 153 (1998) 117-126.
- [27] C. A. Duarte, I. Babuška, J. T. Oden, Generalized finite element method for three-dimensional structural mechanics problems. Computers and Structures 77 (2000) 215-232.
- [28] T. Strouboulis, I. Babuška, K. Copps, The design and analysis of the generalized finite element method. Computer Methods in Applied Mechanics and Engineering 181 (2000) 43-69.
- [29] T. Strouboulis, I. Babuška, K. Copps, The generalized finite element method. Computer Methods in Applied Mechanics and Engineering 190 (2001) 4081-4193.
- [30] C. A. Duarte, D. -J. Kim, D. M. Quaresma, Arbitrarily smooth generalized finite element approximations. Computer Methods in Applied Mechanics and Engineering 196 (2006) 33-56.
- [31] C. A. Duarte, D. Q. Migliano, E. B. Becker, A technique to combine meshfree- and finite element-based partition of unity approximations (Department of Civil and Environmental Engineering - University of Illinois at Urbana-Champaign) Structural Research Series 638 (2005).
- [32] G. R. Liu, Mesh free methods: moving beyond the finite element method, CRC Press, Boca Raton, 2003.
- [33] I. Babuška, G. Caloz, J. E. Osborn, Special finite element methods for a class

- of second order elliptic problems with rough coefficients. SIAM Journal of Numerical Analysis 31 (1994) 945-981.
- [34] J. M. Melenk, On generalized finite element method. Ph.D. dissertation, University of Maryland, 1995.
- [35] J. M. Melenk, I. Babuška, The partition of unity finite element method: basic theory and applications. Computer Methods in Applied Mechanics and Engineering 139 (1996) 289-314.
- [36] I. Babuška, J. M. Melenk, The partition of unity finite element method. International Journal for Numerical Methods in Engineering 40 (1997) 727-758.
- [37] C. A. Duarte, The hp -cloud method. Ph.D dissertation, The University of Texas at Austin, 1996.
- [38] C. A. Duarte, J. T. Oden, An $h-p$ adaptive method using cloud. Computer Methods in Applied Mechanics and Engineering 139 (1996) 237-262.
- [39] T. Belytschko, T. Black, Elastic crack growth in finite elements with minimal remeshing. International Journal for Numerical Methods in Engineering 45 (1999) 601-620.
- [40] P. J. O'Hara, C. A. Duarte, T. Eason, Generalized finite element analysis of three-dimensional heat transfer problems exhibiting sharp thermal gradients. Computer Methods in Applied Mechanics and Engineering 198 (2009) 1857-1871.
- [41] T. Strouboulis, L. Zhang, I. Babuška, Generalized finite element method using mesh-based handbooks: application to problems in domains with many voids.

Computer Methods in Applied Mechanics and Engineering 192 (2003) 3109-3161.

- [42] C. A. Duarte, O. N. Hamzeh, T. J. Liszka, W. W. Tworzydlo, A generalized finite element method for the simulation of three-dimensional crack propagation. Computer Methods in Applied Mechanics and Engineering 190 (2001) 2227-2262.
- [43] F. B. Barros, C. S. Barcellos, C. A. Duarte, $-p$ Adaptive C^k generalized finite element method for arbitrary polygonal clouds. Computational Mechanics 41 (2007) 175-187.
- [44] T. Strouboulis, L. Zhang, D. Wang, I. Babuška, A posteriori error estimation for generalized finite element methods. Computer Methods in Applied Mechanics and Engineering 195 (2006) 852-879.
- [45] P. J. O'Hara, Finite element analysis of three-dimensional heat transfer for problems involving sharp thermal gradients. M.Sc. dissertation, University of Illinois at Urbana-Champaign, 2007.
- [46] C. S. Barcellos, P. T. R. Mendonça, C. A. Duarte, A C^k continuous generalized finite element formulations applied to laminated Kirchhoff plate model. Computational Mechanics 44 (2009) 377-393.
- [47] O. A. Garcia, E. A. Fancello, P. T. R. Mendonça, Developments in the application of the generalized finite element method to thick shell problems. Computational Mechanics 44 (2009) 669-682.
- [48] J. T. Oden, J. N. Reddy, An introduction to the mathematical theory of finite elements, Wiley, New York, 1976.

- [49] J. N. Reddy, Mechanics of laminated composite plates and shells: theory and analysis, CRC Press, Boca Raton, 2004.
- [50] B. Szabó, I. Babuška, Finite element analysis, John Wiley and Sons, New York, 1991.
- [51] S. Vidoli, R. C. Batra, Derivation of plate and rod equations for a piezoelectric body from a mixed three-dimensional variational principle. *Journal of Elasticity* 59 (2000) 23-50.

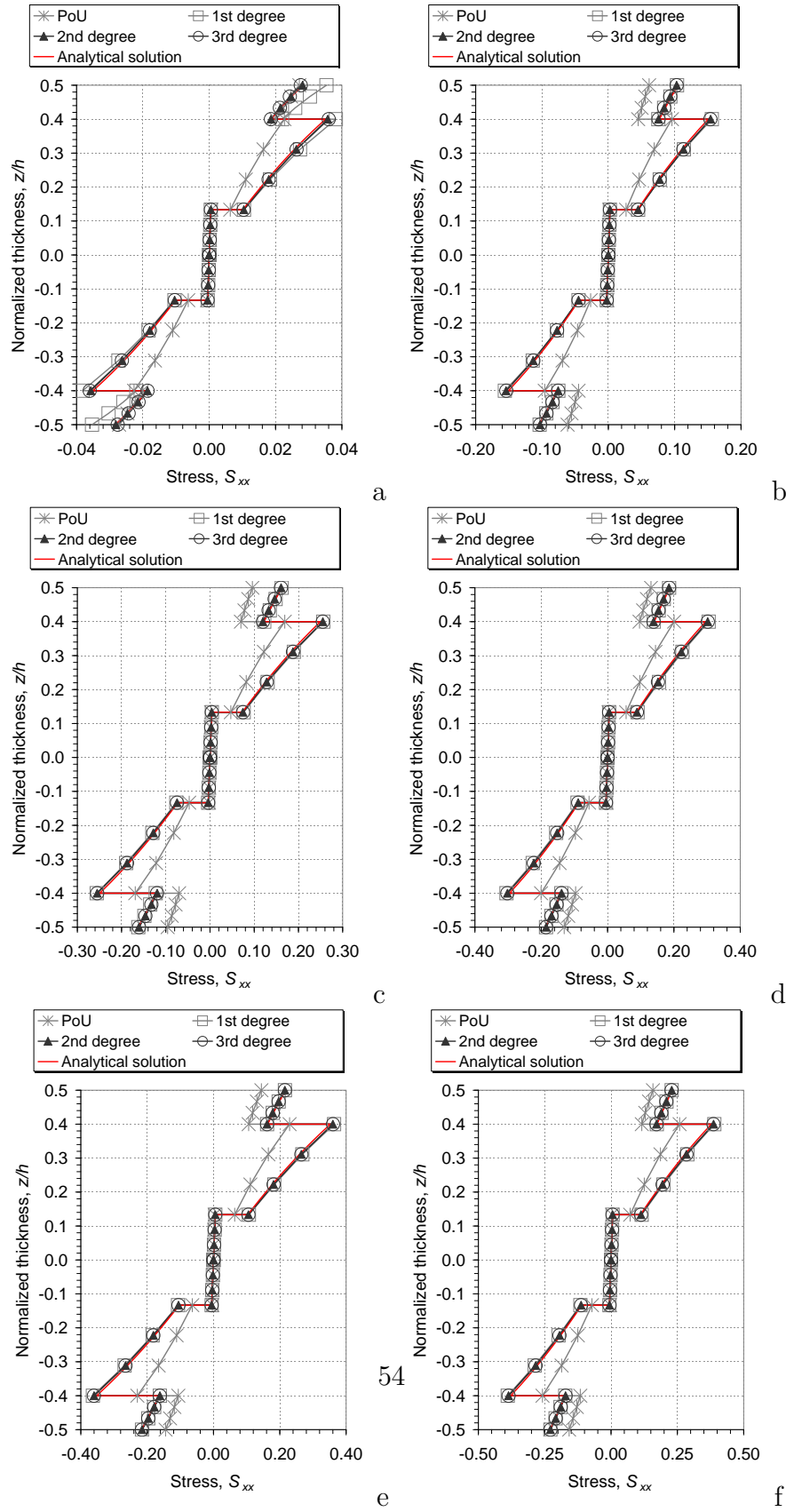


Figure 8: Distribution of non-dimensionalized in-plane stress S_{xx} within the plate thickness, at the points along the line C .

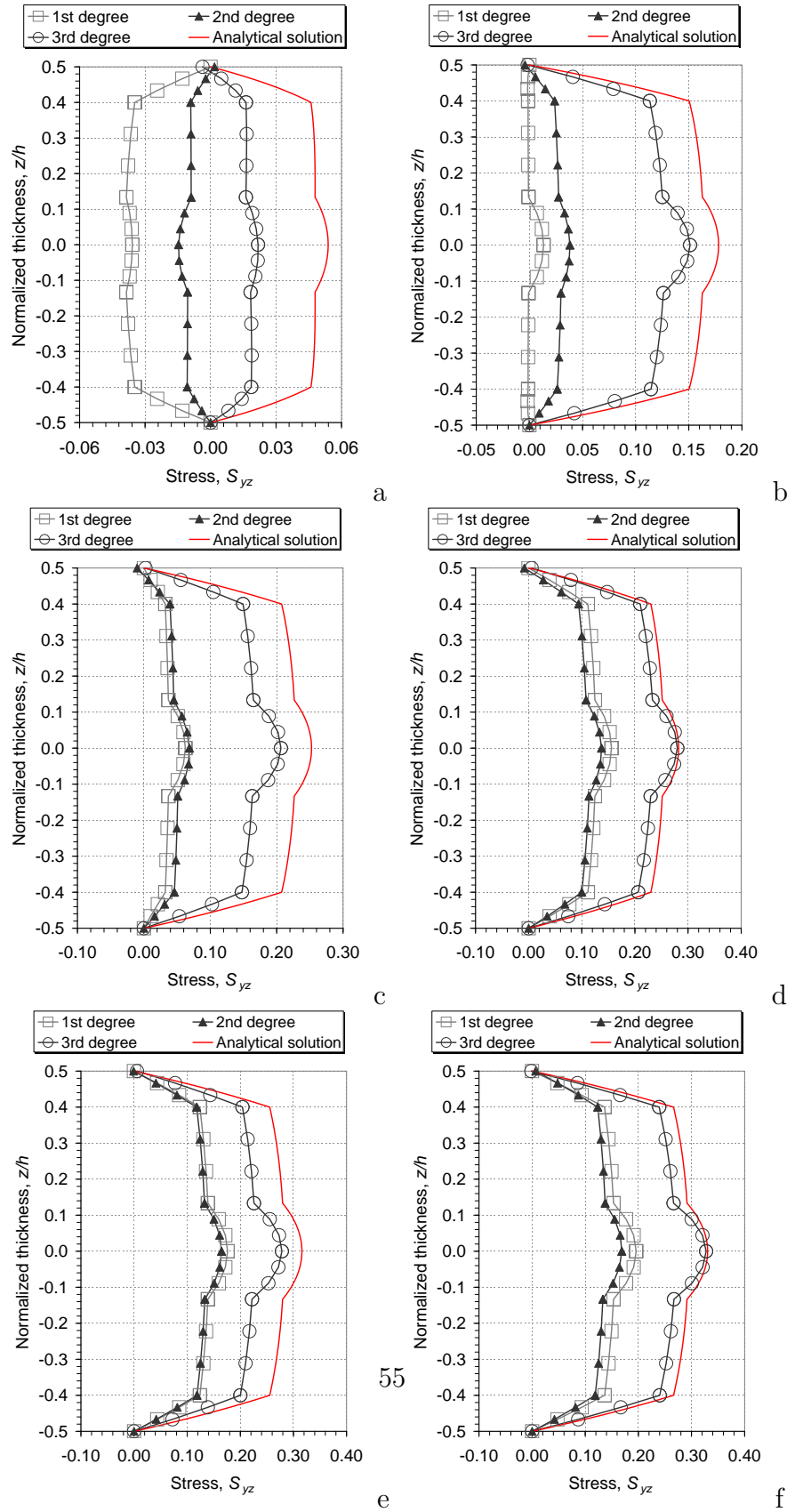


Figure 9: Distribution of non-dimensionalized transversal shear stress S_{yz} within the plate thickness, at the points along the line A.

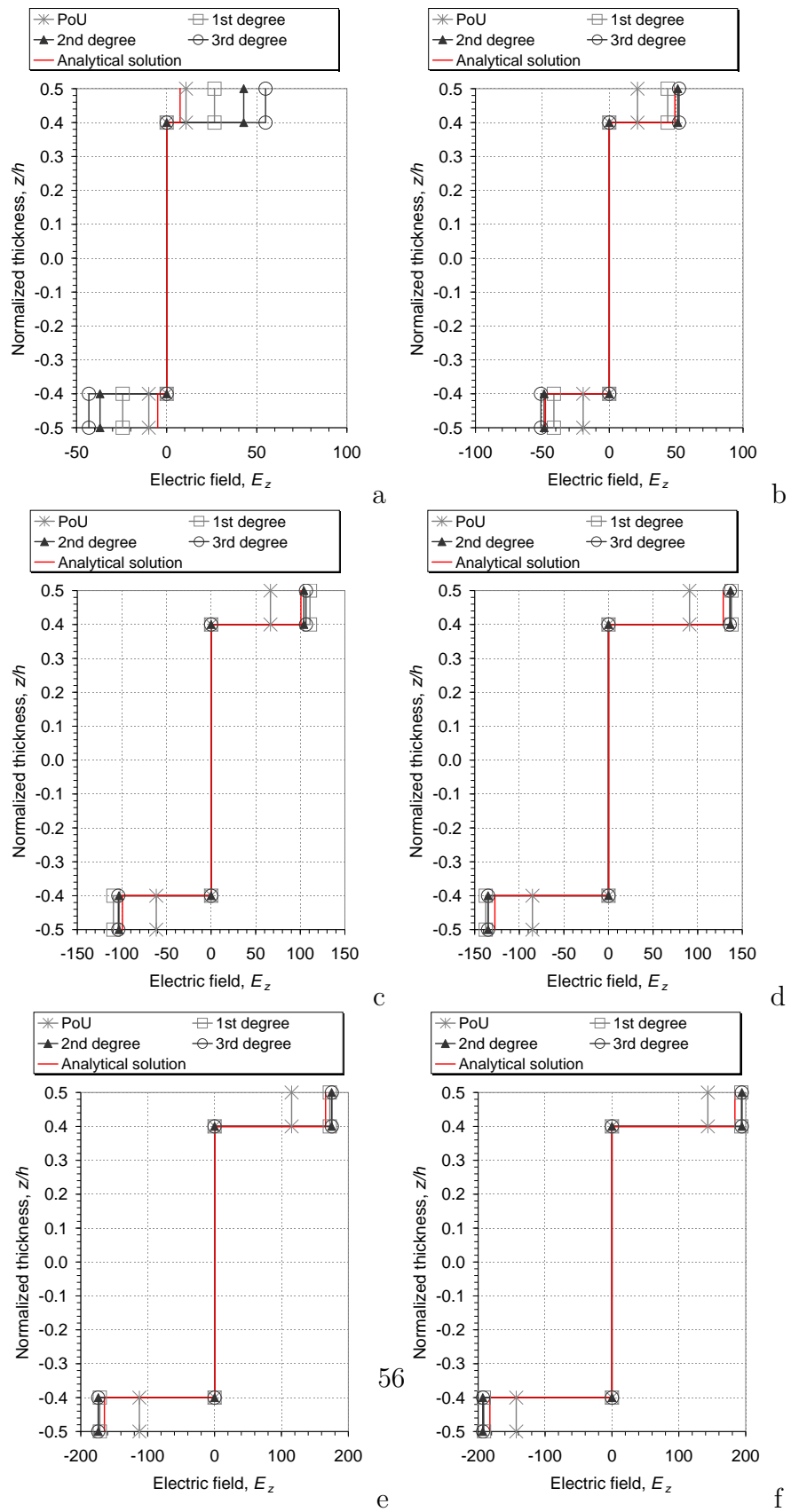
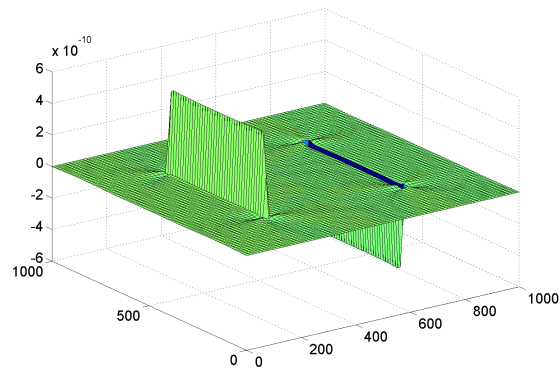
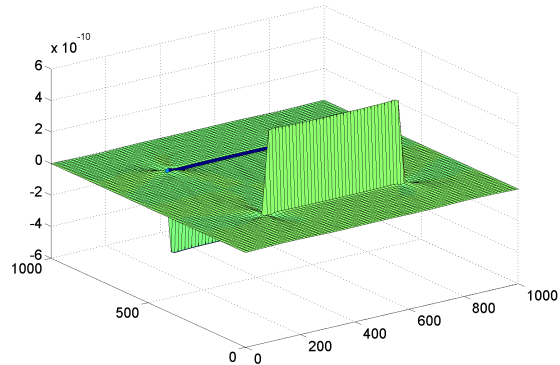


Figure 10: Distribution of electric field within the plate thickness, at the points along the line E .



a



b

Figure 11: Analytical solution for the ψ_{3x} and ψ_{3y} higher order warping variables, a and b respectively, for the thin plate with actuators.

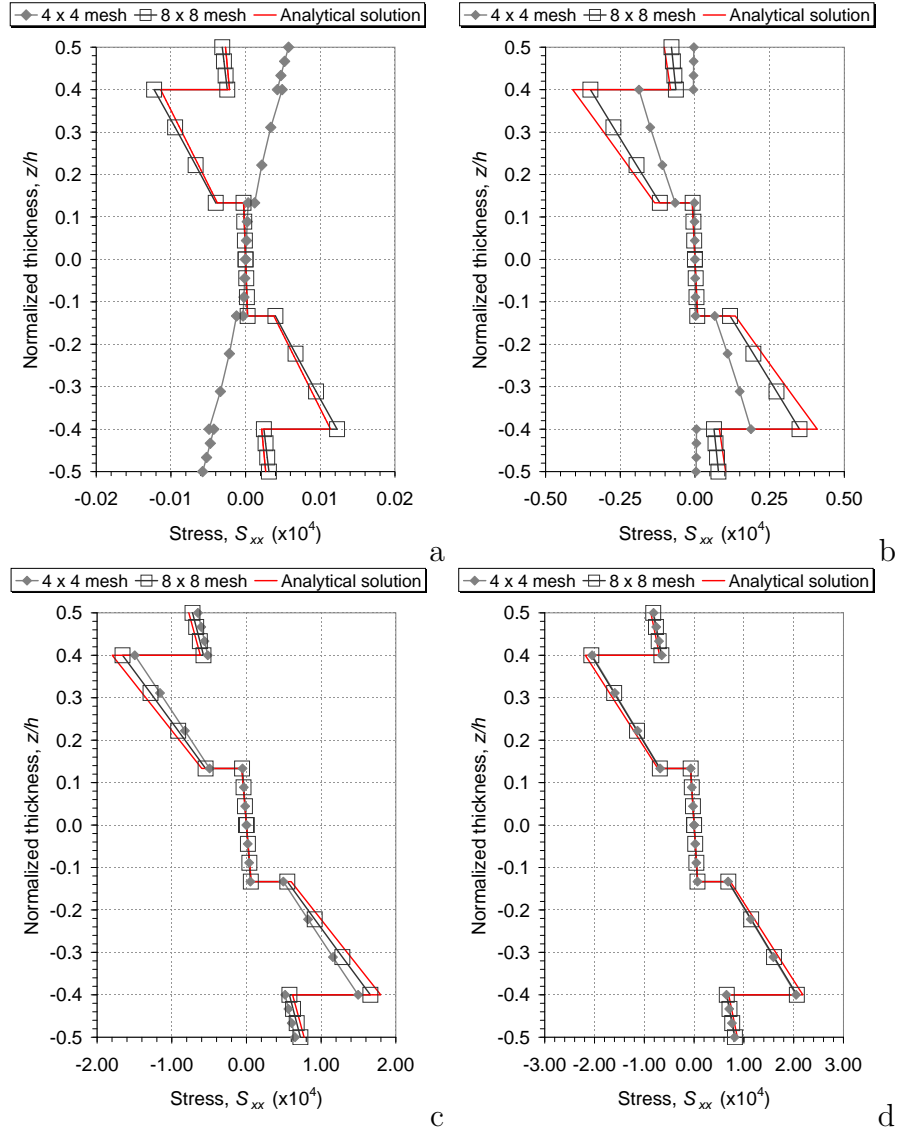


Figure 12: Distribution of non-dimensionalized in-plane stress S_{xx} within the plate thickness, at the points along the line E , considering third degree enrichment.

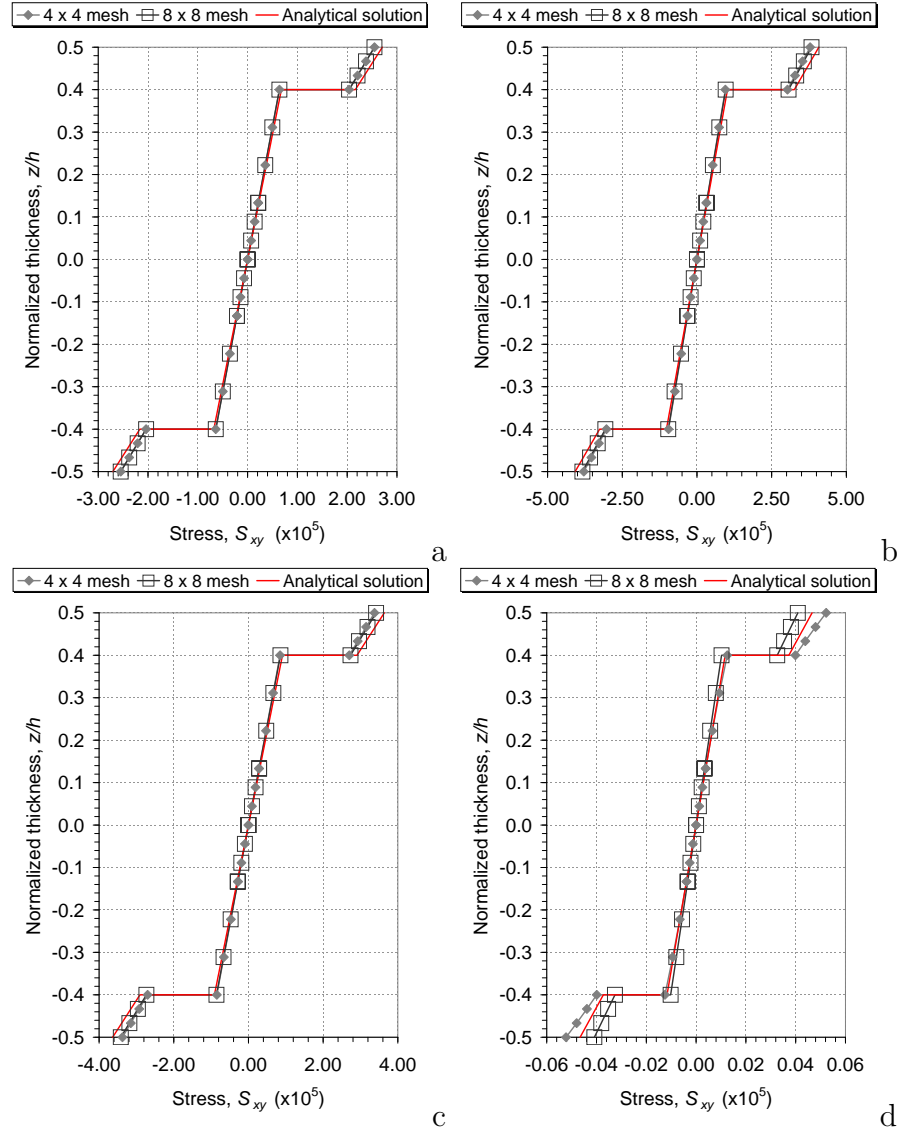


Figure 13: Distribution of non-dimensionalized in-plane shear stress S_{xy} within the plate thickness, at the points along the line E , considering third degree enrichment.

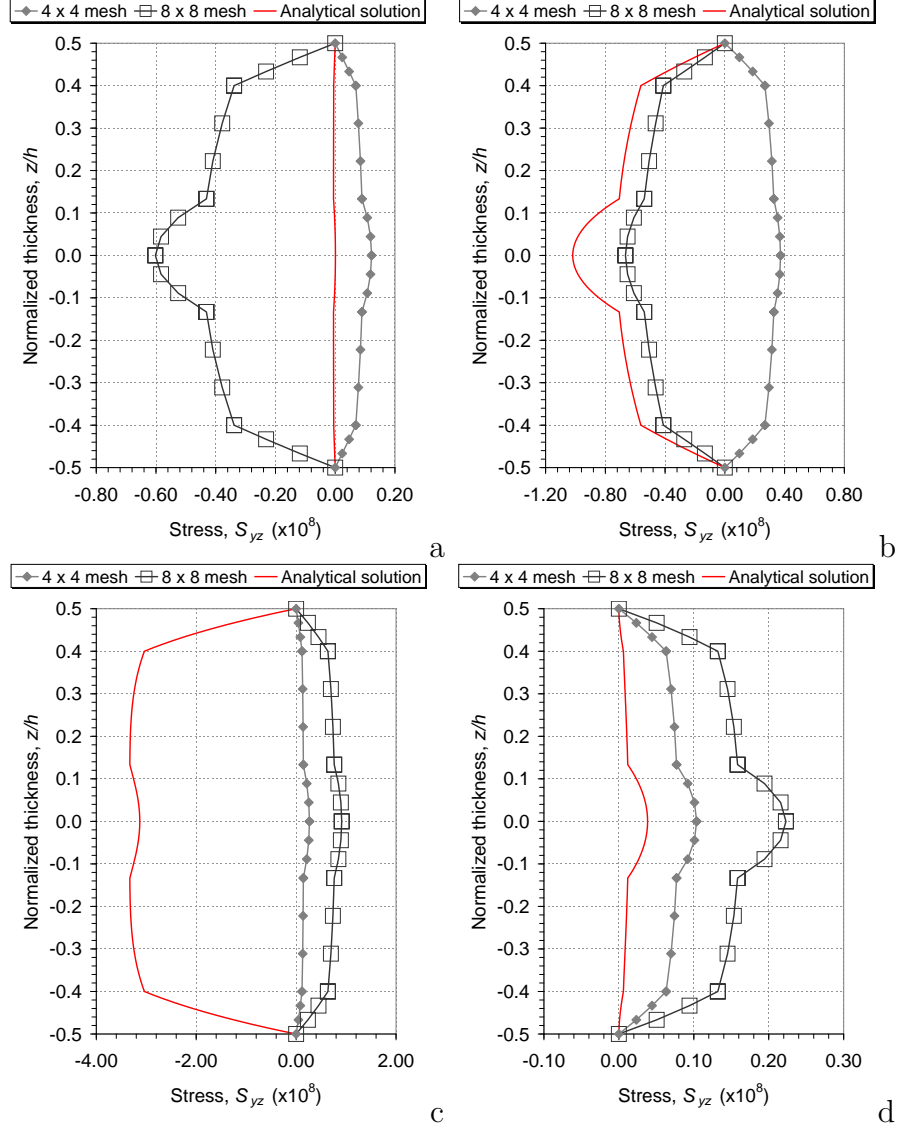


Figure 14: Distribution of non-dimensionalized transversal shear stress S_{yz} within the plate thickness, at the points along the line E , considering third degree enrichment.